5-2012

Theoretical Study on Spontaneous Symmetry Breaking in Strongly Correlated Electrons

Xiaotian Zhang
xzhang25@utk.edu

To the Graduate Council:

I am submitting herewith a dissertation written by Xiaotian Zhang entitled "Theoretical Study on Spontaneous Symmetry Breaking in Strongly Correlated Electrons." I have examined the final electronic copy of this dissertation for form and content and recommend that it be accepted in partial fulfillment of the requirements for the degree of Doctor of Philosophy, with a major in Physics.

Elbio R. Dagotto, Major Professor

We have read this dissertation and recommend its acceptance:

Adriana Moreo, Robert N. Compton, Norman Mannella

Accepted for the Council:
Dixie L. Thompson

Vice Provost and Dean of the Graduate School

(Original signatures are on file with official student records.)

Theoretical Study on Spontaneous Symmetry Breaking in Strongly Correlated Electrons

A Dissertation

Presented for the

Doctor of Philosophy

Degree

The University of Tennessee, Knoxville

Xiaotian Zhang

May 2012

Acknowledgements

I really have enjoyed the time that I stayed at the University of Tennessee, Knoxville and Oak Ridge National Laboratory. It will be one of the most important memories of my life. I have learnt a lot from all the faculties, staffs and students who I have been working with. Here I want to show my special greetings to the following people.

1. My advisor, distinguished professor Elbio Dagotto. *Dr.* Dagotto is a very nice advisor to work with. Unlike many other advisors, *Dr.* Dagotto takes the students' future and lives to be a priority in his considerations and decisions. He teaches his students everything he can, and offers suggestions and help whenever needed. Also, *Dr.* Dagotto never pushes students. He gives students enough time to think deeply into the physics behind the problems and get an good understanding of it. I am very glad that I have such a good advisor during my Ph.D. study.

2. My classical mechanics instructor, professor Yuri Kamyshkov. I have learnt and discussed a lot with *Dr.* Kamyshkov not only about classical mechanics but also particle physics, even life. I could not imagine I would have a russian friend over 60 years old in the United States before I came here, but now it becomes true.

3. My advanced solid state physics instructor, professor Pengcheng Dai. *Dr.* Dai is an experimentalist but he has many collaborations with my theoretical group. His excellent knowledge in experiments helped me a lot to improve my research work. Also, as a Chinese professor, he is very enthusiastic to offer his great help to the Chinese students here, either inside or out of his research group. *Dr.* Dai now also has a position in the institute of physics in Beijing, so hopefully I can still meet him

there in the future when I travel back to China after graduation.

4. My collaborators *Dr.* Shuai Dong and *Dr.* Di Xiao. Shuai Dong was an exchange student in my research group from Nanjing University, China, and now he is a professor at Southeast University, China. Di Xiao is a research staff at Oak Ridge National Laboratory. They taught and helped me in my research work like brothers. From them I learnt a lot about manganites and topological insulators.

5. Although my Ph. D. study is in the United States, there is one gentleman in China that I must show my best appreciation to in this acknowledgements. He is my undergraduate department head, research advisor and solid state physics instructor, professor Bangfen Zhu. He opened the door of condensed matter physics for me by his excellent teaching in the class and perfect research advising. He also recommended me to *Dr.* Dagotto, which helped me to join my current group for my Ph. D. study. I can say that without him I can definitely never be a Ph. D. in physics.

Abstract

In the early days of condensed matter physics, the single electron approximation was considered to be a very good approach in order to explore the properties of many systems. However, as time goes on, a variety of new systems have been discovered and many of them, such as high temperature superconductors and manganites, show phenomenas that evidently can not be explained by single electron theories. Spontaneous symmetry breaking is a very important and famous concept in physics, from the Higgs mechanism in particle physics to the spin density wave in condensed matter physics. The present text describes the detailed studies that the author has done, in order to explore the role of electron-electron interaction induced spontaneous symmetry breaking in two different systems: the iron-pnictides and perovskite [111] bilayers. For the iron-pnictides, we firstly derived the $t-J$ model from the two-orbital Hubbard model in the strong coupling limit. The result is totally different from the famous single-orbital $t-J$ model. Following this model, our group calculated the phase diagram of the iron-pnictides via the Lanczos method.[1] Secondly, we calculated the optical conductivity of the iron-pnictides using the three-orbital Hubbard model under the mean-field approximation and obtained the anisotropy of the optical conductivity which agrees with experiments well. We explained this phenomenon by an effective shift of the Fermi surface induced by electron-electron interaction. For the perovskite [111] bilayers, we used the two-orbital Hubbard model under the mean-field approximation to explore how will the electron-electron

interaction produce a Chern-insulator when a flat band is present, and also how can domain structures be formed by applying doping to a quantum Hall ferromagnet.

Contents

List of Tables

List of Figures

Chapter 1

Introduction

1.1 Iron-Pnictides

The discovery of superconductivity in iron-pnictides has attracted considerable interest in the condensed matter physics community.[2, 3, 4, 5, 6, 7, 8] This new family of compounds includes the "1111" systems (RFeAsO, where R = La, Nd, Sm, Ce...), the "122" systems (AFe_2As_2, where A = Ba, Ca, Sr...), the "111" systems (LiFeAs or NaFeAs), and the "11" systems ($Fe_{1+x}(Te-Se)$ and $Fe_{1+y}Te_{1-x}Se_x$). From the Density Functional Theory (DFT) calculations,[9, 10] the electron-phonon mechanism appears to be too weak to give rise to the high critical temperatures T_c ∼50 K observed in iron-based superconductors, which was also verified by an inelastic neutron scattering experiment.[11] Experimentally, the superconductivity can be observed by doping or by pressurizing the undoped parent compound, which is a (bad) semimetal from the perspective of transport. The highest transition temperature T_c for iron-based superconductors is 56 K and it was observed in $Gd_{1-x}Th_xFeAsO$.[12] This newly discovered family shares many similarities with the cuprates – the first high-T_c superconductors –, such as: both families have layered structures which are Fe-As layers for pnictides and Cu-O layers for cuprates; and both parent compounds are magnetic, with wavevector $(\pi, 0)$ in the case of the pnictides[13, 14] and (π, π) for

the cuprates, in the notation of the square lattice defined by Fe or Cu. However, a significant difference between these two high-T_c superconductors is that the undoped parent compound is a Mott insulator for the cuprates, while it is a (bad) semimetal for the pnictides. This suggests that the regime of a large Hubbard coupling U, widely used in the context of the cuprates, may not be appropriate for a theoretical description of the pnictides. Although Fe-based and Cu-based superconductors have similar layered structures, the mechanisms of electron conduction are vastly different: in the cuprates, electron conduction has to occur primarily via hopping from Cu to O to Cu since O atoms occupy the midpoints of Cu-O-Cu bonds whereas in the Fe-based compounds, while the direct Fe-Fe hopping contributes also, the hopping using As (located in the middle of the elementary square of the Fe lattice) as a bridge is very important. From DFT calculation for Fe-based materials, all five d-orbitals of Fe dominates the bands near the Fermi energy, while As $4p$ orbitals are contributing more to the bands below the Fermi energy.[15] This means that the effective tight-binding model mainly based on the hoppings from Fe to Fe defined on a square lattice involving only the Fe sites is a reasonable starting point.

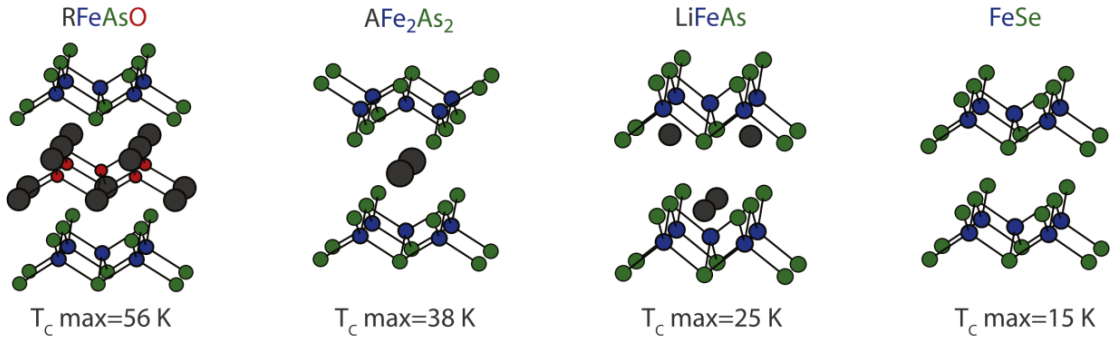

Figure 1.1: Crystal structure of the 1111, 122, 111, and 11 systems. Blue solid balls represent Fe atoms and green ones represent As or Se atoms. Reproduced from Ref [14].

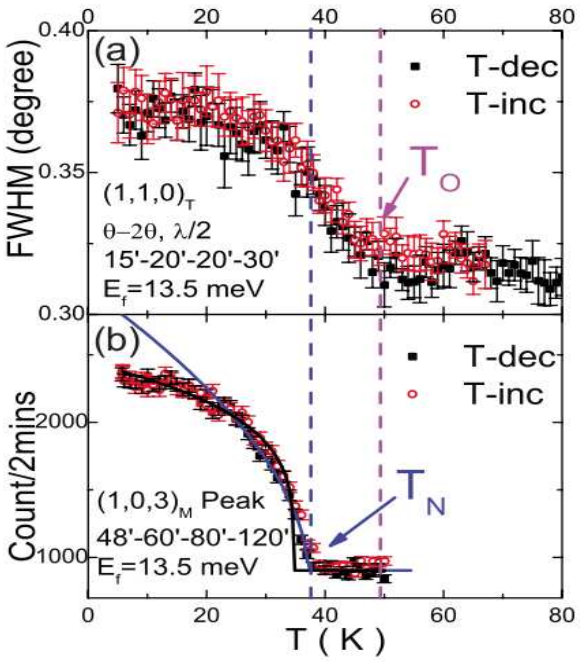

Figure 1.2: Neutron scattering results. (a) Structure transition and (b) magnetic transition for the case of $Na_{1-\delta}FeAs$. Reproduced from Ref [17].

Most of the undoped parent compounds of the iron-based superconductors have similar layered structures. They share the same FeAs layers but with different spacers between two of these FeAs layers for different systems (but no spacer for the 11 systems). Shown in Fig1.1 are the structures of the parent compounds for these four systems[14]: blue solid balls represent the Fe atoms and green ones represent the As or Se atoms. An interesting relation between the optimal transition temperatures and the separation between FeAs layers can be found in Fig 1.1: the materials with higher optimal transition temperature have larger separation between layers, which also sheds some light on how to find new materials with higher T_c, which means that those materials with more space between FeAs layers probably superconduct at a higher temperature. Generally, the crystal structures of these parent compounds are tetragonal at room temperature but become orthorhombic at low temperature. Indeed, the parent compounds undergo a tetragonal to orthorhombic structural

transition accompanied by a magnetic transition which exhibits a SDW state below the transition temperature T_{SDW}. The 111 (Li/NaFeAs) materials were claimed to be very unique since there is neither structural nor magnetic transitions.[16] However, both transitions were found, and with different transition temperatures, with a 1.5% Na deficiency [17] (Fig 1.2). For the 1111 systems, the undoped parent compounds undergo a structural phase transition (from tetragonal (space group P4/nmm) to orthorhombic (space group Cmma)),[18, 19, 20, 21, 22, 23, 24, 25, 26, 27] which some believe to be magnetically driven to relieve magnetic frustration.[13] Indeed the magnetic transition develops slightly below the structural transition temperature, which exhibits spin-density wave (SDW) order below the critical temperature. For the 122 systems, the undoped parent compounds show a structural phase transition from the teragonal I4/mmm space group to the orthorhombic Fmmm space group.[28, 29, 30, 31, 32, 33, 34, 35, 36] A magnetic phase transition to a SDW state occurs at the same critical temperature, which is unlike the 1111 systems. Both of these two transitions appear to be first-order transitions in the 122 systems. However, the structural phase transition is a first-order transition while the magnetic transition is second order for the 1111 materials. For the 11 systems, the structural and magnetic transition occur simultaneously in a first-order transition for the pure Te system.[13]

Material	T_S (K)	T_N(Fe) (K)	μ_{Fe} (μ_B)	q_{Fe}	Spin direction	T_N(R) (K)	μ_R (μ_B)	q_R	Spin direction
LaOFeAs	155	137	0.36	101	Likely *a*	–			
CeOFeAs	158	140	0.8	100	*a*	4.0	0.94	101	*a, b, c*
PrOFeAs	153	127	0.48	100	*a*	14	0.84	100	*c*
NdOFeAs	150	141	0.25	101	Likely *a*	1.96	1.55	100	*a, c*
$CaFe_2As_2$	173	173	0.80	101	*a*	–			
$SrFe_2As_2$	220	220	0.94	101	*a*	–			
$BaFe_2As_2$	142	143	0.87	101	*a*	–			
$Fe_{1.068}Te$	67	67	2.25	100	*b*	–			

Figure 1.3: Information about the structural phase transitions for undoped pnictide materials, including the ordering temperatures, spin configuration, and ordered moment for the iron spins. Reproduced from Ref [13].

The structural phase transition could be driven by magnetic interactions, as the lower symmetry allows the magnetic frustration to be relieved and the system to

order.[13] At low temperature, the magnetic structure within the a-b plane is identical for both 1111 and 122 systems, as shown in Fig 1.4.[13] It consists of chains of Fe spins which are parallel to each other along the shorter b-axis (typical spacing $5.68\mathring{A}$ in LaOFeAs), while the spins are coupled antiferromagnetically along the longer a-axis (typical spacing $5.71\mathring{A}$ in LaOFeAs)[13]. The direction of the spins are along the a-axis. It is impossible for this type of magnetic structure to survive in tetragonal symmetry, which may be the origin of the structural distortion. For the 1111 systems, the spins along the c-axis are coupled either antiferromagnetically as for La and Nd, or ferromagnetically as for Ce and Pr, while for the 122 systems, the spins along the c-axis are antiparallel. The information of the magnetic moments of Fe in some materials are listed in Fig 1.3, as well as the transition temperatures. Typically, the magnetic moment is around 0.5 μ_B for 1111 systems, except for CeFeAsO where it is 0.8 μ_B, whereas that of 122 systems is slightly less than 1.0 μ_B. However, a big difference appears that in the magnetic moment for the "11" systems is around 2.0 μ_B (but note that its wavevector is $(\frac{\pi}{2}, \frac{\pi}{2})$). The relatively small values of the magnetic moments observed for some of the parent compounds also indicate that the AF order is a spin-density-wave (SDW) arising from itinerant electrons in those cases.[8] From the table shown in Fig 1.3, it can be found that all the materials seem to have the spin direction along the a-axis, which supply a method to distinguish the a- from the b-axis. Also, doping can introduce phase transition between the antiferromagnetic phase and the superconducting phase.[23, 37, 38, 39, 40, 41, 42] In some systems those two phases can co-exist while in some others they do not. An experimental phase diagram is shown in Fig 1.5 as an example.

1.2 Perovskite [111] Bilayer

Perovskite structures have been studied by a variety of both theoretical and experimental efforts for a long time as one of the most popular areas in strongly correlated electron systems. The perovskite structure is illustrated in Fig 1.6, panel

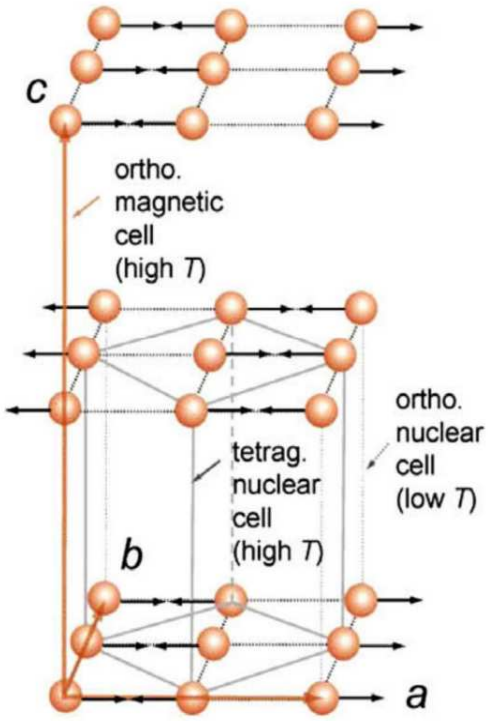

Figure 1.4: Magnetic structure for the iron spins in the 1:1:1:1 and 1:2:2 systems. The in-plane spin configuration and spin direction are identical for all these materials, where the spins are parallel along the orthorhombic b-axis, antiparallel along the a-axis, and with the spin direction along a. This spin arrangement will be of much importance in the discussion of results for the optical conductivity, later in this report. Along the more weakly coupled c-axis the arrangement can be either parallel (ferro) or antiparallel (antiferro). All the structures are simple commensurate magnetic structures. Reproduced from Ref [13].

(a). The lattice is cubic, with a transition metal atom, such as Mn or Ti, at the center of every unit cell. This atom will be surrounded by an oxygen octahedron, and the conners of the cubic are occupied by other metal atoms such as La, Sr or Ca. The seven kinds of possible magnetic structures and their labels are listed in Fig 1.6, panel (b). In fact, many materials of this family show extremely rich phases under different external conditions. Different phases compete with each other strongly, which may produce mixed phases or even more interesting phenomenons, such as phase separation (tendency) and colossal magnetoresistance (CMR).[43]

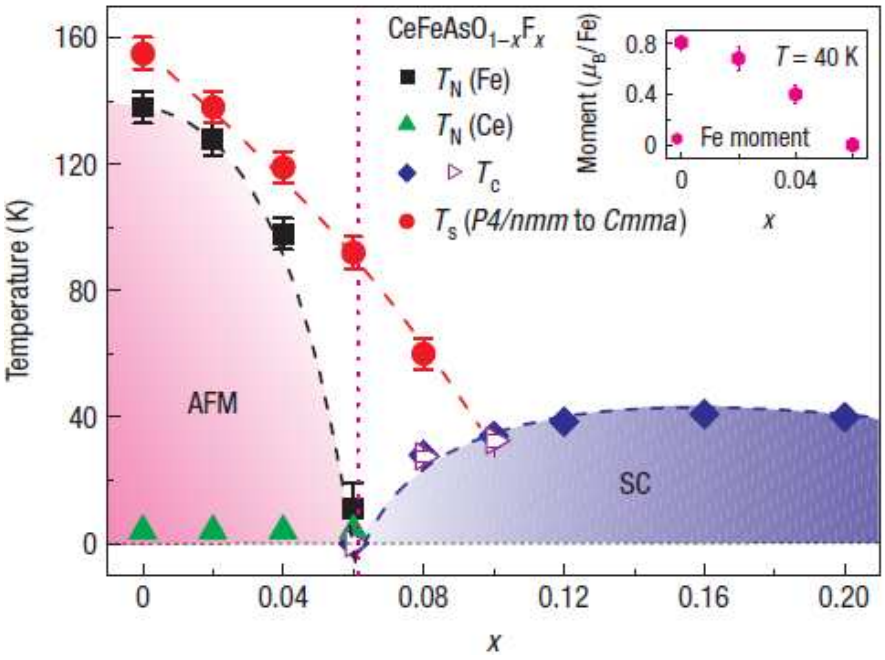

Figure 1.5: Experimental phase diagram of the $CeFeAsO_{1-x}F_x$ system. The antiferromagnetism is completely replaced by superconductivity by F doping. Reproduced from Ref [23].

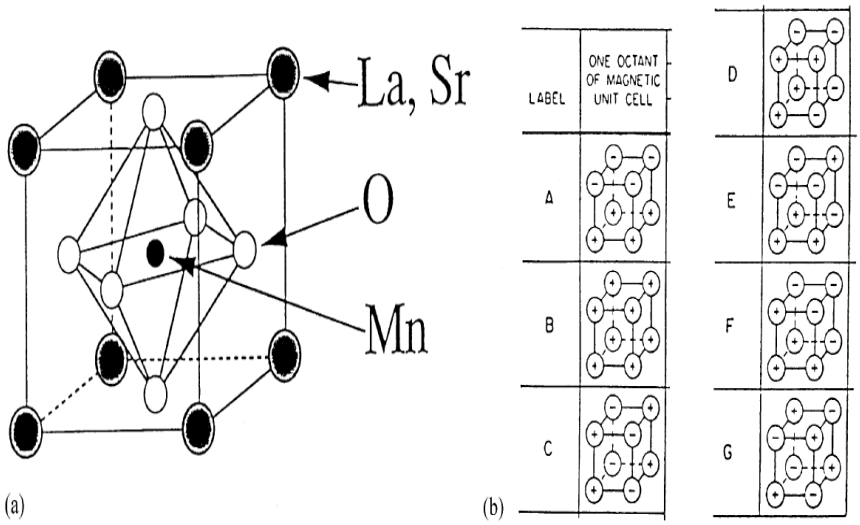

Figure 1.6: Perovskite structure (a) and possible magnetic structures and their labels (b). Reproduced from Ref [44] and Ref [45].

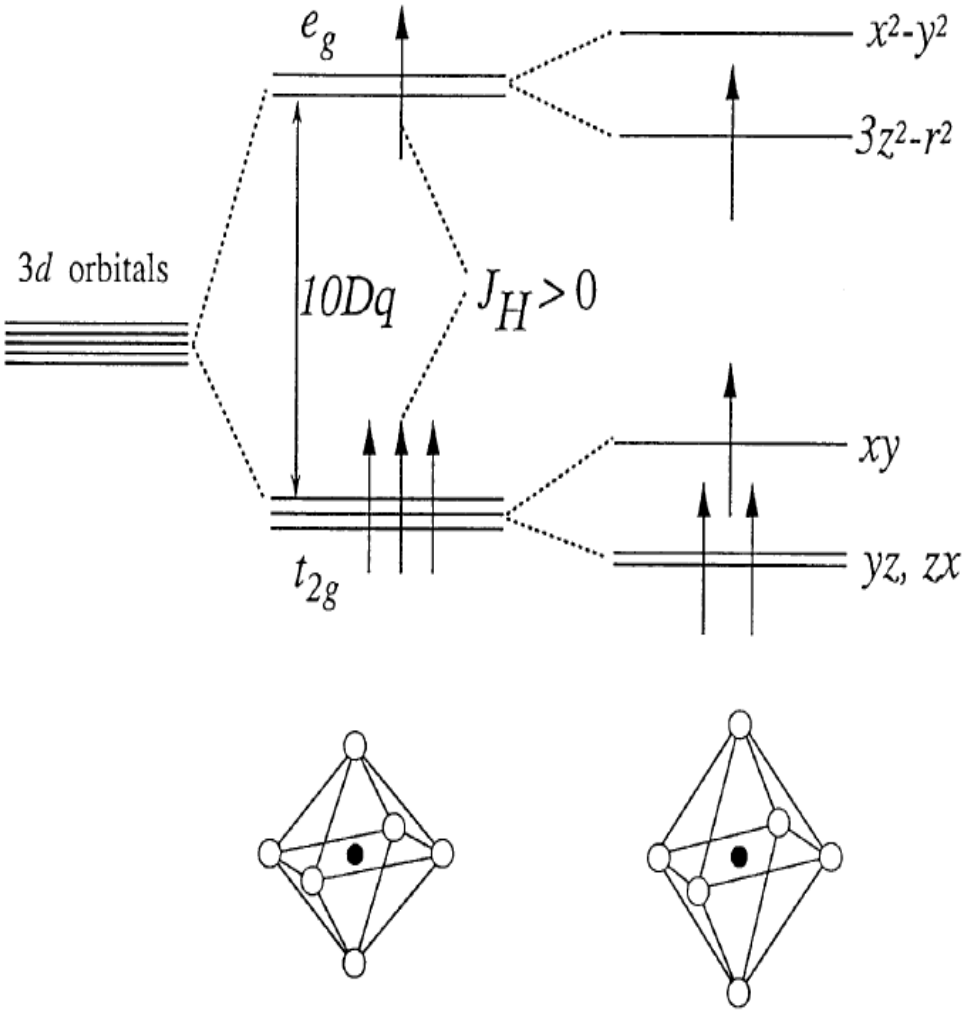

Figure 1.7: Orbital splitting induced by the oxygen octahedron (a) and the Jahn-Teller effect (b). Reproduced from Ref [44].

Due to the repulsion from the negative oxygen ions, the five d orbitals of the transition metal atom, which are degenerate in atomic physics, are not split. d_{xz}, d_{yz} and d_{xy} orbitals now have lower energy and are called t_{2g} orbitals. The rest two orbitals, $d_{3z^2-r^2}$ and $d_{x^2-y^2}$ have higher energy and are called e_g orbitals. Moreover, the t_{2g} and e_g orbitals will get further splitting among themselves due to the displacement of the oxygen ions, which is named as Jahn-Teller effect (Fig 1.7).

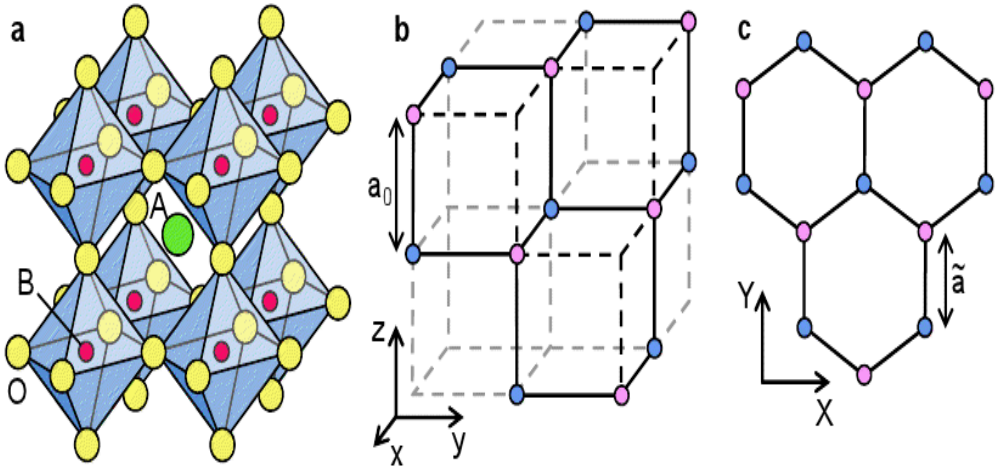

Figure 1.8: The perovskite structure (a) is cubic but its [111] bilayer (b) and (c) appears to be hexagonal. Reproduced from Ref [56].

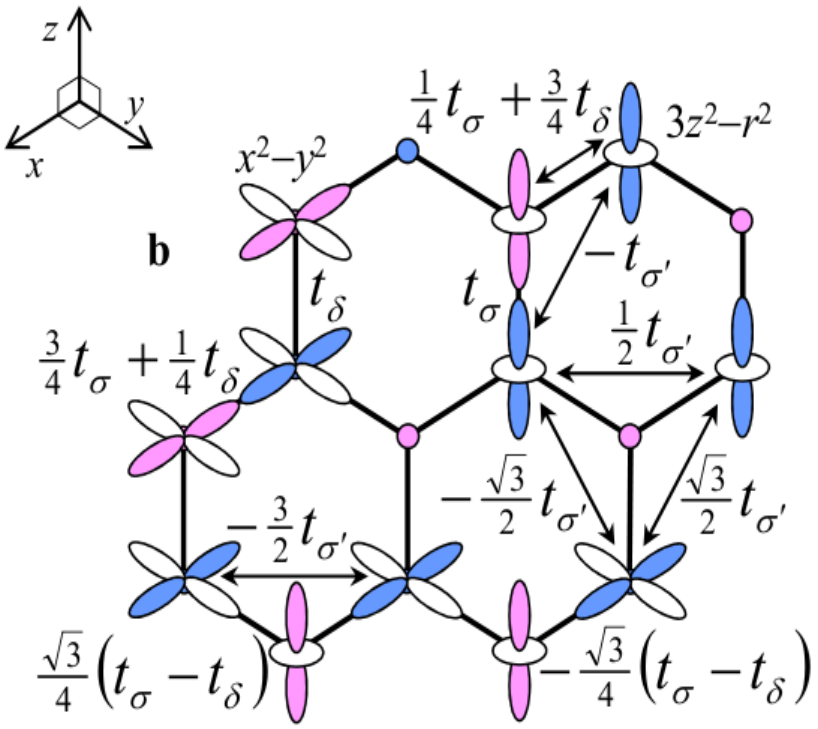

Figure 1.9: Proveskite [111] bilayer hopping among t_{2g} (a) and e_g (b) orbitals. Reproduced from Ref [56].

Different from the cubic symmetry shown above, perovskite [111] bilayer appears to be a hexagonal lattice seen from the top (Fig 1.8). The interesting physics in hexagonal lattices has been studied a lot in the past. Haldane firstly pointed out that such symmetry allows a non-zero Hall conductance in the absence of an external magnetic field,[46] which implies non-trivial topology in similar band insulators. Following Haldane, many efforts, both theoretically[47, 48, 49, 50] and experimentally,[51, 52, 53, 54, 55] have been made in order to explore a family of materials called topological insulators, which always have strong spin-orbital coupling. We know that in the presence of an external magnetic field, the canonical momentum $\mathbf{p}$ becomes $\mathbf{p}_0 + e\mathbf{A}$, where $\mathbf{p_0}$ is the mechanical momentum corresponding to the classical $m\mathbf{v}$, e is the electron charge and $\mathbf{A}$ is the vector potential of the external magnetic field. However, the kinetic energy part in the Hamiltonian should still be

$$\frac{\mathbf{p}_0^2}{2m} = \frac{(\mathbf{p} - e\mathbf{A})^2}{2m}, \tag{1.1}$$

and hence the Hamiltonian will get an extra term proportional to $\mathbf{A} \cdot \mathbf{p}$. In the presence of spin-orbital coupling which is proportional to

$$\begin{aligned} \mathbf{l} \cdot \mathbf{s} &= (\mathbf{r} \times \mathbf{p}) \cdot \mathbf{s} \\ &= (\mathbf{s} \times \mathbf{r}) \cdot \mathbf{p}, \end{aligned} \tag{1.2}$$

we have an effective vector potential $\mathbf{A}_{eff} = \mathbf{s} \times \mathbf{r}$, which makes the quantum Hall effect to be possible.

So far, the physically realized materials of topological insulators are only narrow band-gap semiconductors based on Hg or Bi, in which the electrons close to the Fermi surface belong to s and p orbitals. In perovskite materials, the dominating electrons are e_g d electrons, which may open a new page for the topological insulator study. However, we see from the expression of $\mathbf{A}_{eff}$ that spin-up and spin-down electrons feel opposite effective magnetic fields and the spin-orbital coupling of those orbitals does not split spin-up and spin-down electrons. Hence unless we can find some other

mechanism to produce magnetism, there will be equal amount of spin-up and spin-down electrons in the ground state so that they will produce zero net electric current (but non-zero net spin current). In other words, we need a magnet to obtain the quantum Hall effect in the e_g electrons. For the perovskite [111] bilayers the hopping among t_{2g} and e_g orbitals are shown in Fig 1.9. Fortunately, band structure calculation shows that two flat bands exist for the e_g electrons as shown in Fig 1.10.[56] Because of the flatness, the band will be extremely sensitive to an external magnetic field: if a band is absolutely flat, an arbitrarily small uniform magnetic field should be able to make the system to be completely ferromagnetic when the band is half-filled.

Up to now only single-electron physics is considered, and my research described in Chapter 3 will discuss how the electron-electron interaction will modify such systems.

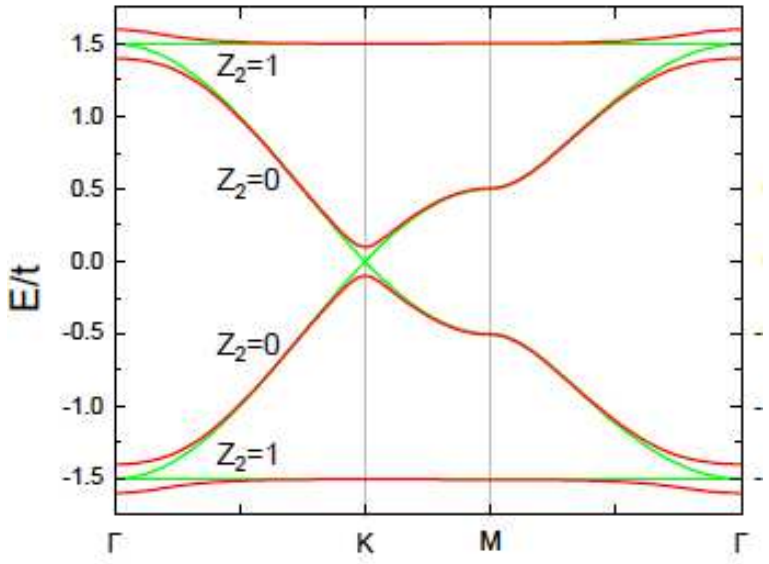

Figure 1.10: The perovskite [111] bilayer energy band in the e_g model. When there is no spin-orbital coupling (green curve) the lowest and highest bands are absolutely flat and the bands touch each other quadratically at the Γ point. After a small spin-orbital coupling is introduced (red curve) the flat bands get dispersion and a gap is opened at the Γ point. Reproduced from Ref [56].

1.3 Multi-orbital Hubbard Model and Mean-field Approximation

1.3.1 *Total Hamiltonian*

In the Hubbard model, the total Hamiltonian is $H = H_{\rm TB} + H_{\rm int}$. The first term is the tight-binding term $H_{\rm TB}$:

$$H_{\rm TB} = \sum_{<\mathbf{i},\mathbf{j}>} \sum_{\alpha,\beta,\sigma} t_{ij}^{\alpha\beta} (c_{\mathbf{i},\alpha,\sigma}^{\dagger} c_{\mathbf{j},\beta,\sigma} + h.c.), \tag{1.3}$$

where $c_{\mathbf{i},\alpha,\sigma}^{\dagger}$ creates an electron with spin σ in the orbital α of site $\mathbf{i}$, and $t_{ij}^{\alpha\beta}$ refers to the tunneling amplitude of a particle hopping from orbital α at site $\mathbf{i}$ to orbital β at site $\mathbf{j}$. The second term is the Coulombic on-site interaction $H_{\rm int}$:

$$\begin{aligned} H_{\rm int} &= H_1 + H_2 + H_3 + H_4 \\ &= U \sum_{\mathbf{i},\alpha} n_{\mathbf{i},\alpha,\uparrow} n_{\mathbf{i},\alpha,\downarrow} \\ &\quad + (U' - \frac{J}{2}) \sum_{\mathbf{i},\alpha<\beta} n_{\mathbf{i},\alpha} n_{\mathbf{i},\beta} \\ &\quad - 2J \sum_{\mathbf{i},\alpha<\beta} \mathbf{S}_{\mathbf{i},\alpha} \cdot \mathbf{S}_{\mathbf{i},\beta} \\ &\quad + J \sum_{\mathbf{i},\alpha<\beta} (c_{\mathbf{i},\alpha,\uparrow}^{\dagger} c_{\mathbf{i},\alpha,\downarrow}^{\dagger} c_{\mathbf{i},\beta,\downarrow} c_{\mathbf{i},\beta,\uparrow} + h.c.), \end{aligned} \tag{1.4}$$

where $\mathbf{S}_{\mathbf{i},\alpha}$ ($n_{\mathbf{i},\alpha}$) is the spin (charge density) of orbital α at site $\mathbf{i}$, and $n_{\mathbf{i},\alpha} = n_{\mathbf{i},\alpha,\uparrow} + n_{\mathbf{i},\alpha,\downarrow}$. These terms refer to, respectively, an on-site intra-orbital Hubbard repulsion characterized by U (H_1), an inter-orbital repulsion characterized by $U^{'}$ (H_2), a finite Hund coupling characterized by J (H_3), and a "pair-hopping" term characterized also by J (H_4). The relation $U' = U - 2J$ between the Kanamori parameters has been used here for simplicity. All of the following studies will be

based on this multi-orbital Hubbard model.

1.3.2 *Hartree-Fock Approximation*

The Hartree-Fock (HF) approximation is a type of mean-field approximation that includes two parts: Hartree terms and Fock terms. In the Hartree-Fock approximation, these operators can be replaced by a mean value using the identity:

$$c^{\dagger}_{\mathbf{i},\alpha,\sigma}c_{\mathbf{i}',\alpha',\sigma'} = \langle c^{\dagger}_{\mathbf{i},\alpha,\sigma}c_{\mathbf{i}',\alpha',\sigma'}\rangle + (c^{\dagger}_{\mathbf{i},\alpha,\sigma}c_{\mathbf{i}',\alpha',\sigma'} - \langle c^{\dagger}_{\mathbf{i},\alpha,\sigma}c_{\mathbf{i}',\alpha',\sigma'}\rangle),$$

where, if $\alpha = \alpha^{'}$ and $\sigma = \sigma^{'}$, the second part has two terms both on the same position (diagonal element) of the Hamiltonian matrix and substituting each other, so that the second term should be very small and can be recognized as fluctuation at low temperature. While $\alpha = \alpha^{'}$ and $\sigma = \sigma^{'}$ can not be valid simultaneously, the second part has one off-diagonal term and the other diagonal term, so that it can never be recognized as small fluctuation. However, at low temperature, the configuration on each site is very stable, so that the first part becomes really small.

Following this argument, the first term (H_1) in the interaction (H_{int}), which is the on-site intra-orbital Hubbard repulsion, which gives the energy cost of having two electrons located in the same orbital at the same site, can be written in the Hartree approximation as:

$$\begin{aligned}
H_1^H &= U\sum_{\mathbf{i},\alpha} n_{\mathbf{i},\alpha,\uparrow}n_{\mathbf{i},\alpha,\downarrow} \\
&= U\sum_{\mathbf{i},\alpha}(\langle n_{\mathbf{i},\alpha,\uparrow}\rangle + n_{\mathbf{i},\alpha,\uparrow} - \langle n_{\mathbf{i},\alpha,\uparrow}\rangle) \times (\langle n_{\mathbf{i},\alpha,\downarrow}\rangle + n_{\mathbf{i},\alpha,\downarrow} - \langle n_{\mathbf{i},\alpha,\downarrow}\rangle) \\
&= U\sum_{\mathbf{i},\alpha}(n_{\mathbf{i},\alpha,\uparrow}\langle n_{\mathbf{i},\alpha,\downarrow}\rangle + n_{\mathbf{i},\alpha,\downarrow}\langle n_{\mathbf{i},\alpha,\uparrow}\rangle - \langle n_{\mathbf{i},\alpha,\uparrow}\rangle\langle n_{\mathbf{i},\alpha,\downarrow}\rangle + (n_{\mathbf{i},\alpha,\uparrow} - \langle n_{\mathbf{i},\alpha,\uparrow}\rangle) \times (n_{\mathbf{i},\alpha,\downarrow} - \langle n_{\mathbf{i},\alpha,\downarrow}\rangle)),
\end{aligned}$$

where the second order term is small at low temperature, and in the Fock approximation it can be written as:

$$
\begin{aligned}
H_1^F &= -U\sum_{\mathbf{i},\alpha}(c^\dagger_{\mathbf{i},\alpha,\uparrow}c_{\mathbf{i},\alpha,\downarrow})(c^\dagger_{\mathbf{i},\alpha,\downarrow}c_{\mathbf{i},\alpha,\uparrow}) \\
&= -U\sum_{\mathbf{i},\alpha}(\langle c^\dagger_{\mathbf{i},\alpha,\uparrow}c_{\mathbf{i},\alpha,\downarrow}\rangle + c^\dagger_{\mathbf{i},\alpha,\uparrow}c_{\mathbf{i},\alpha,\downarrow} - \langle c^\dagger_{\mathbf{i},\alpha,\uparrow}c_{\mathbf{i},\alpha,\downarrow}\rangle) \times (\langle c^\dagger_{\mathbf{i},\alpha,\downarrow}c_{\mathbf{i},\alpha,\uparrow}\rangle + c^\dagger_{\mathbf{i},\alpha,\downarrow}c_{\mathbf{i},\alpha,\uparrow} - \langle c^\dagger_{\mathbf{i},\alpha,\downarrow}c_{\mathbf{i},\alpha,\uparrow}\rangle) \\
&= -U\sum_{\mathbf{i},\alpha}(\langle c^\dagger_{\mathbf{i},\alpha,\uparrow}c_{\mathbf{i},\alpha,\downarrow}\rangle c^\dagger_{\mathbf{i},\alpha,\downarrow}c_{\mathbf{i},\alpha,\uparrow} + \langle c^\dagger_{\mathbf{i},\alpha,\downarrow}c_{\mathbf{i},\alpha,\uparrow}\rangle c^\dagger_{\mathbf{i},\alpha,\uparrow}c_{\mathbf{i},\alpha,\downarrow} - \langle c^\dagger_{\mathbf{i},\alpha,\uparrow}c_{\mathbf{i},\alpha,\downarrow}\rangle\langle c^\dagger_{\mathbf{i},\alpha,\downarrow}c_{\mathbf{i},\alpha,\uparrow}\rangle \\
&\qquad + (c^\dagger_{\mathbf{i},\alpha,\uparrow}c_{\mathbf{i},\alpha,\downarrow} - \langle c^\dagger_{\mathbf{i},\alpha,\uparrow}c_{\mathbf{i},\alpha,\downarrow}\rangle) \times (c^\dagger_{\mathbf{i},\alpha,\downarrow}c_{\mathbf{i},\alpha,\uparrow} - \langle c^\dagger_{\mathbf{i},\alpha,\downarrow}c_{\mathbf{i},\alpha,\uparrow}\rangle)).
\end{aligned}
$$

We are searching for a Hamiltonian in which, at least at low temperature, it is a good enough approximation for us too keep only the quadratic terms, in order to avoid using many body basis in the calculation. In the Hartree Hamiltonian, the quartic terms are small ones, while in the Fock Hamiltonian the quadratic terms are small, so that should be approximately equal to the quartic term in H^H. In the Hartree-Fock approximation, we add the quadratic terms of H_1^H and H_1^F together and write:

$$
\begin{aligned}
H_1 &= U\sum_{\mathbf{i},\alpha} n_{\mathbf{i},\alpha,\uparrow}n_{\mathbf{i},\alpha,\downarrow} \\
&= U\sum_{\mathbf{i},\alpha} c^\dagger_{\mathbf{i},\alpha,\uparrow}c_{\mathbf{i},\alpha,\uparrow}c^\dagger_{\mathbf{i},\alpha,\downarrow}c_{\mathbf{i},\alpha,\downarrow} \\
&\approx U\sum_{\mathbf{i},\alpha}(n_{\mathbf{i},\alpha,\uparrow}\langle n_{\mathbf{i},\alpha,\downarrow}\rangle + n_{\mathbf{i},\alpha,\downarrow}\langle n_{\mathbf{i},\alpha,\uparrow}\rangle - \langle n_{\mathbf{i},\alpha,\uparrow}\rangle\langle n_{\mathbf{i},\alpha,\downarrow}\rangle) \\
&- U\sum_{\mathbf{i},\alpha}(\langle c^\dagger_{\mathbf{i},\alpha,\uparrow}c_{\mathbf{i},\alpha,\downarrow}\rangle c^\dagger_{\mathbf{i},\alpha,\downarrow}c_{\mathbf{i},\alpha,\uparrow} + \langle c^\dagger_{\mathbf{i},\alpha,\downarrow}c_{\mathbf{i},\alpha,\uparrow}\rangle c^\dagger_{\mathbf{i},\alpha,\uparrow}c_{\mathbf{i},\alpha,\downarrow} - \langle c^\dagger_{\mathbf{i},\alpha,\uparrow}c_{\mathbf{i},\alpha,\downarrow}\rangle\langle c^\dagger_{\mathbf{i},\alpha,\downarrow}c_{\mathbf{i},\alpha,\uparrow}\rangle).
\end{aligned}
$$

The second term (H_2) represents one part of the inter-orbital Hubbard repulsion, which gives the energy cost $U-2J$ of having two electrons located in different orbitals at the same site. Following the same procedure as for H_1, the Hartree-Fock approximation to H_2 reads:

$$
\begin{aligned}
H_2 &= (U' - \frac{J}{2}) \sum_{\mathbf{i},\alpha<\beta} n_{\mathbf{i},\alpha} n_{\mathbf{i},\beta} \\
&= (U' - \frac{J}{2}) \sum_{\mathbf{i},\alpha<\beta} (n_{\mathbf{i},\alpha,\uparrow} + n_{\mathbf{i},\alpha,\downarrow})(n_{\mathbf{i},\beta,\uparrow} + n_{\mathbf{i},\beta,\downarrow}) \\
&= (U' - \frac{J}{2}) \sum_{\mathbf{i},\alpha<\beta} (c^\dagger_{\mathbf{i},\alpha,\uparrow} c_{\mathbf{i},\alpha,\uparrow} c^\dagger_{\mathbf{i},\beta,\uparrow} c_{\mathbf{i},\beta,\uparrow} + c^\dagger_{\mathbf{i},\alpha,\uparrow} c_{\mathbf{i},\alpha,\uparrow} c^\dagger_{\mathbf{i},\beta,\downarrow} c_{\mathbf{i},\beta,\downarrow} \\
&\qquad + c^\dagger_{\mathbf{i},\alpha,\downarrow} c_{\mathbf{i},\alpha,\downarrow} c^\dagger_{\mathbf{i},\beta,\uparrow} c_{\mathbf{i},\beta,\uparrow} + c^\dagger_{\mathbf{i},\alpha,\downarrow} c_{\mathbf{i},\alpha,\downarrow} c^\dagger_{\mathbf{i},\beta,\downarrow} c_{\mathbf{i},\beta,\downarrow}) \\
&\approx (U' - \frac{J}{2}) \sum_{\mathbf{i},\alpha<\beta} [(n_{\mathbf{i},\alpha,\uparrow} + n_{\mathbf{i},\alpha,\downarrow})(\langle n_{\mathbf{i},\beta,\uparrow}\rangle + \langle n_{\mathbf{i},\beta,\downarrow}\rangle) \\
&\qquad + (n_{\mathbf{i},\beta,\uparrow} + n_{\mathbf{i},\beta,\downarrow})(\langle n_{\mathbf{i},\alpha,\uparrow}\rangle + \langle n_{\mathbf{i},\alpha,\downarrow}\rangle) \\
&\qquad - \langle n_{\mathbf{i},\alpha,\uparrow}\rangle(\langle n_{\mathbf{i},\beta,\uparrow}\rangle + \langle n_{\mathbf{i},\beta,\downarrow}\rangle)] \\
&\quad -(U' - \frac{J}{2}) \sum_{\mathbf{i},\alpha<\beta} [(\langle c^\dagger_{\mathbf{i},\alpha,\uparrow} c_{\mathbf{i},\beta,\uparrow}\rangle c^\dagger_{\mathbf{i},\beta,\uparrow} c_{\mathbf{i},\alpha,\uparrow} + \langle c^\dagger_{\mathbf{i},\beta,\uparrow} c_{\mathbf{i},\alpha,\uparrow}\rangle c^\dagger_{\mathbf{i},\alpha,\uparrow} c_{\mathbf{i},\beta,\uparrow} \\
&\qquad - \langle c^\dagger_{\mathbf{i},\alpha,\uparrow} c_{\mathbf{i},\beta,\uparrow}\rangle \langle c^\dagger_{\mathbf{i},\beta,\uparrow} c_{\mathbf{i},\alpha,\uparrow}\rangle) \\
&\qquad + (\langle c^\dagger_{\mathbf{i},\alpha,\uparrow} c_{\mathbf{i},\beta,\downarrow}\rangle c^\dagger_{\mathbf{i},\beta,\downarrow} c_{\mathbf{i},\alpha,\uparrow} + \langle c^\dagger_{\mathbf{i},\beta,\downarrow} c_{\mathbf{i},\alpha,\uparrow}\rangle c^\dagger_{\mathbf{i},\alpha,\uparrow} c_{\mathbf{i},\beta,\downarrow} \\
&\qquad - \langle c^\dagger_{\mathbf{i},\alpha,\uparrow} c_{\mathbf{i},\beta,\downarrow}\rangle \langle c^\dagger_{\mathbf{i},\beta,\downarrow} c_{\mathbf{i},\alpha,\uparrow}\rangle) \\
&\qquad + (\langle c^\dagger_{\mathbf{i},\alpha,\downarrow} c_{\mathbf{i},\beta,\uparrow}\rangle c^\dagger_{\mathbf{i},\beta,\uparrow} c_{\mathbf{i},\alpha,\downarrow} + \langle c^\dagger_{\mathbf{i},\beta,\uparrow} c_{\mathbf{i},\alpha,\downarrow}\rangle c^\dagger_{\mathbf{i},\alpha,\downarrow} c_{\mathbf{i},\beta,\uparrow} \\
&\qquad - \langle c^\dagger_{\mathbf{i},\alpha,\downarrow} c_{\mathbf{i},\beta,\uparrow}\rangle \langle c^\dagger_{\mathbf{i},\beta,\uparrow} c_{\mathbf{i},\alpha,\downarrow}\rangle) \\
&\qquad + (\langle c^\dagger_{\mathbf{i},\alpha,\downarrow} c_{\mathbf{i},\beta,\downarrow}\rangle c^\dagger_{\mathbf{i},\beta,\downarrow} c_{\mathbf{i},\alpha,\downarrow} + \langle c^\dagger_{\mathbf{i},\beta,\downarrow} c_{\mathbf{i},\alpha,\downarrow}\rangle c^\dagger_{\mathbf{i},\alpha,\downarrow} c_{\mathbf{i},\beta,\downarrow} \\
&\qquad - \langle c^\dagger_{\mathbf{i},\alpha,\downarrow} c_{\mathbf{i},\beta,\downarrow}\rangle \langle c^\dagger_{\mathbf{i},\beta,\downarrow} c_{\mathbf{i},\alpha,\downarrow}\rangle)].
\end{aligned}
\tag{1.5}
$$

The third term (H_3) represents the spin-dependent part of the inter-orbital Hubbard repulsion. When two electrons have a symmetric spin wave function, their spacial wave function must be anti-symmetric so that they have less possibility to be close to each other. For this reason, this term, which is often called Hund coupling term, favors the ferromagnetic (FM) alignment of the spins in different orbitals (α, β) at the same lattice site $(\mathbf{i})$. The Hartree-Fock approximation to H_3 reads:

$$
\begin{aligned}
H_3 &= -2J \sum_{\mathbf{i},\alpha<\beta} \mathbf{S}_{\mathbf{i},\alpha} \cdot \mathbf{S}_{\mathbf{i},\beta} \\
&= -\frac{J}{2} \sum_{\mathbf{i},\alpha<\beta} [(c^\dagger_{\mathbf{i},\alpha,\uparrow} c_{\mathbf{i},\alpha,\downarrow} + c^\dagger_{\mathbf{i},\alpha,\downarrow} c_{\mathbf{i},\alpha,\uparrow})(c^\dagger_{\mathbf{i},\beta,\uparrow} c_{\mathbf{i},\beta,\downarrow} + c^\dagger_{\mathbf{i},\beta,\downarrow} c_{\mathbf{i},\beta,\uparrow}) \\
&\qquad +(-i\, c^\dagger_{\mathbf{i},\alpha,\uparrow} c_{\mathbf{i},\alpha,\downarrow} + i\, c^\dagger_{\mathbf{i},\alpha,\downarrow} c_{\mathbf{i},\alpha,\uparrow})(-i\, c^\dagger_{\mathbf{i},\beta,\uparrow} c_{\mathbf{i},\beta,\downarrow} + i\, c^\dagger_{\mathbf{i},\beta,\downarrow} c_{\mathbf{i},\beta,\uparrow}) \\
&\qquad +(c^\dagger_{\mathbf{i},\alpha,\uparrow} c_{\mathbf{i},\alpha,\uparrow} - c^\dagger_{\mathbf{i},\alpha,\downarrow} c_{\mathbf{i},\alpha,\downarrow})(c^\dagger_{\mathbf{i},\beta,\uparrow} c_{\mathbf{i},\beta,\uparrow} - c^\dagger_{\mathbf{i},\beta,\downarrow} c_{\mathbf{i},\beta,\downarrow})] \\
&\approx -\frac{J}{2} \sum_{\mathbf{i},\alpha<\beta} [2(\langle c^\dagger_{\mathbf{i},\alpha,\uparrow} c_{\mathbf{i},\alpha,\downarrow}\rangle c^\dagger_{\mathbf{i},\beta,\downarrow} c_{\mathbf{i},\beta,\uparrow} + \langle c^\dagger_{\mathbf{i},\beta,\downarrow} c_{\mathbf{i},\beta,\uparrow}\rangle c^\dagger_{\mathbf{i},\alpha,\uparrow} c_{\mathbf{i},\alpha,\downarrow} - \langle c^\dagger_{\mathbf{i},\alpha,\uparrow} c_{\mathbf{i},\alpha,\downarrow}\rangle \langle c^\dagger_{\mathbf{i},\beta,\downarrow} c_{\mathbf{i},\beta,\uparrow}\rangle) \\
&\qquad +2(\langle c^\dagger_{\mathbf{i},\alpha,\downarrow} c_{\mathbf{i},\alpha,\uparrow}\rangle c^\dagger_{\mathbf{i},\beta,\uparrow} c_{\mathbf{i},\beta,\downarrow} + \langle c^\dagger_{\mathbf{i},\beta,\uparrow} c_{\mathbf{i},\beta,\downarrow}\rangle c^\dagger_{\mathbf{i},\alpha,\downarrow} c_{\mathbf{i},\alpha,\uparrow} - \langle c^\dagger_{\mathbf{i},\alpha,\downarrow} c_{\mathbf{i},\alpha,\uparrow}\rangle \langle c^\dagger_{\mathbf{i},\beta,\uparrow} c_{\mathbf{i},\beta,\downarrow}\rangle) \\
&\qquad +(\langle c^\dagger_{\mathbf{i},\alpha,\uparrow} c_{\mathbf{i},\alpha,\uparrow}\rangle c^\dagger_{\mathbf{i},\beta,\uparrow} c_{\mathbf{i},\beta,\uparrow} + \langle c^\dagger_{\mathbf{i},\beta,\uparrow} c_{\mathbf{i},\beta,\uparrow}\rangle c^\dagger_{\mathbf{i},\alpha,\uparrow} c_{\mathbf{i},\alpha,\uparrow} - \langle c^\dagger_{\mathbf{i},\alpha,\uparrow} c_{\mathbf{i},\alpha,\uparrow}\rangle \langle c^\dagger_{\mathbf{i},\beta,\uparrow} c_{\mathbf{i},\beta,\uparrow}\rangle) \\
&\qquad -(\langle c^\dagger_{\mathbf{i},\alpha,\downarrow} c_{\mathbf{i},\alpha,\downarrow}\rangle c^\dagger_{\mathbf{i},\beta,\uparrow} c_{\mathbf{i},\beta,\uparrow} + \langle c^\dagger_{\mathbf{i},\beta,\uparrow} c_{\mathbf{i},\beta,\uparrow}\rangle c^\dagger_{\mathbf{i},\alpha,\downarrow} c_{\mathbf{i},\alpha,\downarrow} - \langle c^\dagger_{\mathbf{i},\alpha,\downarrow} c_{\mathbf{i},\alpha,\downarrow}\rangle \langle c^\dagger_{\mathbf{i},\beta,\uparrow} c_{\mathbf{i},\beta,\uparrow}\rangle) \\
&\qquad -(\langle c^\dagger_{\mathbf{i},\alpha,\uparrow} c_{\mathbf{i},\alpha,\uparrow}\rangle c^\dagger_{\mathbf{i},\beta,\downarrow} c_{\mathbf{i},\beta,\downarrow} + \langle c^\dagger_{\mathbf{i},\beta,\downarrow} c_{\mathbf{i},\beta,\downarrow}\rangle c^\dagger_{\mathbf{i},\alpha,\uparrow} c_{\mathbf{i},\alpha,\uparrow} - \langle c^\dagger_{\mathbf{i},\alpha,\uparrow} c_{\mathbf{i},\alpha,\uparrow}\rangle \langle c^\dagger_{\mathbf{i},\beta,\downarrow} c_{\mathbf{i},\beta,\downarrow}\rangle) \\
&\qquad +(\langle c^\dagger_{\mathbf{i},\alpha,\downarrow} c_{\mathbf{i},\alpha,\downarrow}\rangle c^\dagger_{\mathbf{i},\beta,\downarrow} c_{\mathbf{i},\beta,\downarrow} + \langle c^\dagger_{\mathbf{i},\beta,\downarrow} c_{\mathbf{i},\beta,\downarrow}\rangle c^\dagger_{\mathbf{i},\alpha,\downarrow} c_{\mathbf{i},\alpha,\downarrow} - \langle c^\dagger_{\mathbf{i},\alpha,\downarrow} c_{\mathbf{i},\alpha,\downarrow}\rangle \langle c^\dagger_{\mathbf{i},\beta,\downarrow} c_{\mathbf{i},\beta,\downarrow}\rangle)] \\
&\quad +\frac{J}{2} \sum_{\mathbf{i},\alpha<\beta} [2(\langle c^\dagger_{\mathbf{i},\alpha,\uparrow} c_{\mathbf{i},\beta,\uparrow}\rangle c^\dagger_{\mathbf{i},\beta,\downarrow} c_{\mathbf{i},\alpha,\downarrow} + \langle c^\dagger_{\mathbf{i},\beta,\downarrow} c_{\mathbf{i},\alpha,\downarrow}\rangle c^\dagger_{\mathbf{i},\alpha,\uparrow} c_{\mathbf{i},\beta,\uparrow} - \langle c^\dagger_{\mathbf{i},\alpha,\uparrow} c_{\mathbf{i},\beta,\uparrow}\rangle \langle c^\dagger_{\mathbf{i},\beta,\downarrow} c_{\mathbf{i},\alpha,\downarrow}\rangle) \\
&\qquad +2(\langle c^\dagger_{\mathbf{i},\alpha,\downarrow} c_{\mathbf{i},\beta,\downarrow}\rangle c^\dagger_{\mathbf{i},\beta,\uparrow} c_{\mathbf{i},\alpha,\uparrow} + \langle c^\dagger_{\mathbf{i},\beta,\uparrow} c_{\mathbf{i},\alpha,\uparrow}\rangle c^\dagger_{\mathbf{i},\alpha,\downarrow} c_{\mathbf{i},\beta,\downarrow} - \langle c^\dagger_{\mathbf{i},\alpha,\downarrow} c_{\mathbf{i},\beta,\downarrow}\rangle \langle c^\dagger_{\mathbf{i},\beta,\uparrow} c_{\mathbf{i},\alpha,\uparrow}\rangle) \\
&\qquad +(\langle c^\dagger_{\mathbf{i},\alpha,\uparrow} c_{\mathbf{i},\beta,\uparrow}\rangle c^\dagger_{\mathbf{i},\beta,\uparrow} c_{\mathbf{i},\alpha,\uparrow} + \langle c^\dagger_{\mathbf{i},\beta,\uparrow} c_{\mathbf{i},\alpha,\uparrow}\rangle c^\dagger_{\mathbf{i},\alpha,\uparrow} c_{\mathbf{i},\beta,\uparrow} - \langle c^\dagger_{\mathbf{i},\alpha,\uparrow} c_{\mathbf{i},\beta,\uparrow}\rangle \langle c^\dagger_{\mathbf{i},\beta,\uparrow} c_{\mathbf{i},\alpha,\uparrow}\rangle) \\
&\qquad -(\langle c^\dagger_{\mathbf{i},\alpha,\downarrow} c_{\mathbf{i},\beta,\uparrow}\rangle c^\dagger_{\mathbf{i},\beta,\uparrow} c_{\mathbf{i},\alpha,\downarrow} + \langle c^\dagger_{\mathbf{i},\beta,\uparrow} c_{\mathbf{i},\alpha,\downarrow}\rangle c^\dagger_{\mathbf{i},\alpha,\downarrow} c_{\mathbf{i},\beta,\uparrow} - \langle c^\dagger_{\mathbf{i},\alpha,\downarrow} c_{\mathbf{i},\beta,\uparrow}\rangle \langle c^\dagger_{\mathbf{i},\beta,\uparrow} c_{\mathbf{i},\alpha,\downarrow}\rangle) \\
&\qquad -(\langle c^\dagger_{\mathbf{i},\alpha,\uparrow} c_{\mathbf{i},\beta,\downarrow}\rangle c^\dagger_{\mathbf{i},\beta,\downarrow} c_{\mathbf{i},\alpha,\uparrow} + \langle c^\dagger_{\mathbf{i},\beta,\downarrow} c_{\mathbf{i},\alpha,\uparrow}\rangle c^\dagger_{\mathbf{i},\alpha,\uparrow} c_{\mathbf{i},\beta,\downarrow} - \langle c^\dagger_{\mathbf{i},\alpha,\uparrow} c_{\mathbf{i},\beta,\downarrow}\rangle \langle c^\dagger_{\mathbf{i},\beta,\downarrow} c_{\mathbf{i},\alpha,\uparrow}\rangle) \\
&\qquad +(\langle c^\dagger_{\mathbf{i},\alpha,\downarrow} c_{\mathbf{i},\beta,\downarrow}\rangle c^\dagger_{\mathbf{i},\beta,\downarrow} c_{\mathbf{i},\alpha,\downarrow} + \langle c^\dagger_{\mathbf{i},\beta,\downarrow} c_{\mathbf{i},\alpha,\downarrow}\rangle c^\dagger_{\mathbf{i},\alpha,\downarrow} c_{\mathbf{i},\beta,\downarrow} - \langle c^\dagger_{\mathbf{i},\alpha,\downarrow} c_{\mathbf{i},\beta,\downarrow}\rangle \langle c^\dagger_{\mathbf{i},\beta,\downarrow} c_{\mathbf{i},\alpha,\downarrow}\rangle).
\end{aligned}
\tag{1.6}
$$

The forth term (H_4) is a "pair-hopping" term, which represents two particles with different spins hopping between different orbitals (α, β) at the same lattice site. The Hartree-Fock approximation to H_4 reads:

$$
\begin{aligned}
H_4 &= J\sum_{\mathbf{i},\alpha<\beta} \quad (c^\dagger_{\mathbf{i},\alpha,\uparrow}c^\dagger_{\mathbf{i},\alpha,\downarrow}c_{\mathbf{i},\beta,\downarrow}c_{\mathbf{i},\beta,\uparrow} + h.c.), \\
&\approx J\sum_{\mathbf{i},\alpha<\beta} \quad [-(\langle c^\dagger_{\mathbf{i},\alpha,\uparrow}c_{\mathbf{i},\beta,\downarrow}\rangle c^\dagger_{\mathbf{i},\alpha,\downarrow}c_{\mathbf{i},\beta,\uparrow} + \langle c^\dagger_{\mathbf{i},\alpha,\downarrow}c_{\mathbf{i},\beta,\uparrow}\rangle c^\dagger_{\mathbf{i},\alpha,\uparrow}c_{\mathbf{i},\beta,\downarrow} - \langle c^\dagger_{\mathbf{i},\alpha,\uparrow}c_{\mathbf{i},\beta,\downarrow}\rangle\langle c^\dagger_{\mathbf{i},\alpha,\downarrow}c_{\mathbf{i},\beta,\uparrow}\rangle) \\
&\qquad -(\langle c^\dagger_{\mathbf{i},\beta,\uparrow}c_{\mathbf{i},\alpha,\downarrow}\rangle c^\dagger_{\mathbf{i},\beta,\downarrow}c_{\mathbf{i},\alpha,\uparrow} + \langle c^\dagger_{\mathbf{i},\beta,\downarrow}c_{\mathbf{i},\alpha,\uparrow}\rangle c^\dagger_{\mathbf{i},\beta,\uparrow}c_{\mathbf{i},\alpha,\downarrow} - \langle c^\dagger_{\mathbf{i},\beta,\uparrow}c_{\mathbf{i},\alpha,\downarrow}\rangle\langle c^\dagger_{\mathbf{i},\beta,\downarrow}c_{\mathbf{i},\alpha,\uparrow}\rangle)] \\
&\quad +J\sum_{\mathbf{i},\alpha<\beta} \quad [(\langle c^\dagger_{\mathbf{i},\alpha,\uparrow}c_{\mathbf{i},\beta,\uparrow}\rangle c^\dagger_{\mathbf{i},\alpha,\downarrow}c_{\mathbf{i},\beta,\downarrow} + \langle c^\dagger_{\mathbf{i},\alpha,\downarrow}c_{\mathbf{i},\beta,\downarrow}\rangle c^\dagger_{\mathbf{i},\alpha,\uparrow}c_{\mathbf{i},\beta,\uparrow} - \langle c^\dagger_{\mathbf{i},\alpha,\uparrow}c_{\mathbf{i},\beta,\uparrow}\rangle\langle c^\dagger_{\mathbf{i},\alpha,\downarrow}c_{\mathbf{i},\beta,\downarrow}\rangle) \\
&\qquad +(\langle c^\dagger_{\mathbf{i},\beta,\downarrow}c_{\mathbf{i},\alpha,\downarrow}\rangle c^\dagger_{\mathbf{i},\beta,\uparrow}c_{\mathbf{i},\alpha,\uparrow} + \langle c^\dagger_{\mathbf{i},\beta,\uparrow}c_{\mathbf{i},\alpha,\uparrow}\rangle c^\dagger_{\mathbf{i},\beta,\downarrow}c_{\mathbf{i},\alpha,\downarrow} - \langle c^\dagger_{\mathbf{i},\beta,\downarrow}c_{\mathbf{i},\alpha,\downarrow}\rangle\langle c^\dagger_{\mathbf{i},\beta,\uparrow}c_{\mathbf{i},\alpha,\uparrow}\rangle)],
\end{aligned}
\tag{1.7}
$$

In this HF Hamiltonian, the various expectation values (such as $\langle c^\dagger_{\mathbf{i},\alpha,\uparrow}c_{\mathbf{i},\alpha,\downarrow}\rangle$) are considered as HF parameters and can be determined self-consistently by minimizing the HF energy with respect to the various expectation values numerically.

1.3.3 *Mean-field Approximation in Real Space*

The mean-field approximation employed in this subsection only contains the Hartree terms in the HF approximation. That is, using a reasonable Ansatz it can be proposed as :

$$
\langle c^\dagger_{\mathbf{i},\alpha,\sigma}c_{\mathbf{i}',\alpha',\sigma'}\rangle = \frac{1}{2}(n_\alpha + \sigma m_\alpha e^{i\,\mathbf{Q}\cdot\mathbf{i}})\delta_{\mathbf{i}\mathbf{i}'}\delta_{\alpha\alpha'}\delta_{\sigma\sigma'}, \tag{1.8}
$$

where $\mathbf{Q} = (\pi, 0)$ represents the ordering wave vector of the magnetic order for the parent compounds of pnictides. n_α and m_α are mean-field parameters (to be determined self-consistently) describing the charge density and magnetization of the orbital α, respectively. Only $\langle n_{\mathbf{i},\alpha,\sigma}\rangle$ survives as:

$$
\langle n_{\mathbf{i},\alpha,\uparrow}\rangle = \frac{1}{2}(n_\alpha + m_\alpha e^{i\,\mathbf{Q}\cdot\mathbf{i}}), \tag{1.9}
$$

$$
\langle n_{\mathbf{i},\alpha,\downarrow}\rangle = \frac{1}{2}(n_\alpha - m_\alpha e^{i\,\mathbf{Q}\cdot\mathbf{i}}). \tag{1.10}
$$

It is reasonable to assume that all the other mean values are zero, such as $\langle c^{\dagger}_{\mathbf{i},\alpha,\uparrow} c_{\mathbf{i},\alpha,\downarrow}\rangle = \langle c^{\dagger}_{\mathbf{i},\alpha,\downarrow} c_{\mathbf{i},\alpha,\uparrow}\rangle = 0$, because the possibility of one particle hopping between different orbitals or with different sites or different spins is expected to be small compared to that between the same orbital with same spin. Based on the Hartree approximation results derived above, and plugging in the Ansatz, H_1, H_2, H_3 and H_4 can be rewritten as:

$$\begin{aligned}
H_1 &= U\sum_{\mathbf{i},\alpha}[\frac{1}{2}n_{\mathbf{i},\alpha,\uparrow}(n_\alpha - m_\alpha e^{i\,\mathbf{Q}\cdot\mathbf{i}}) + \frac{1}{2}n_{\mathbf{i},\alpha,\downarrow}(n_\alpha + m_\alpha e^{i\,\mathbf{Q}\cdot\mathbf{i}}) \\
&\quad -\frac{1}{4}(n_\alpha + m_\alpha e^{i\,\mathbf{Q}\cdot\mathbf{i}})(n_\alpha - m_\alpha e^{i\,\mathbf{Q}\cdot\mathbf{i}})] \\
&= -UN\sum_{\alpha}\frac{1}{4}(n_\alpha^2 - m_\alpha^2) + U\sum_{\mathbf{i},\alpha}\frac{1}{2}[n_\alpha(n_{\mathbf{i},\alpha,\uparrow} + n_{\mathbf{i},\alpha,\downarrow}) \\
&\quad +m_\alpha e^{i\,\mathbf{Q}\cdot\mathbf{i}}(n_{\mathbf{i},\alpha,\downarrow} - n_{\mathbf{i},\alpha,\uparrow})], \\
H_2 &= (U' - \frac{J}{2})\sum_{\mathbf{i},\alpha<\beta}[(n_{\mathbf{i},\alpha,\uparrow} + n_{\mathbf{i},\alpha,\downarrow}) \times \frac{1}{2}(n_\beta + m_\beta e^{i\,\mathbf{Q}\cdot\mathbf{i}} + n_\beta - m_\beta e^{i\,\mathbf{Q}\cdot\mathbf{i}}) \\
&\qquad +(n_{\mathbf{i},\beta,\uparrow} + n_{\mathbf{i},\beta,\downarrow}) \times \frac{1}{2}(n_\alpha + m_\alpha e^{i\,\mathbf{Q}\cdot\mathbf{i}} + n_\alpha - m_\alpha e^{i\,\mathbf{Q}\cdot\mathbf{i}}) \\
&\qquad -\frac{1}{2}(n_\alpha + m_\alpha e^{i\,\mathbf{Q}\cdot\mathbf{i}} + n_\alpha - m_\alpha e^{i\,\mathbf{Q}\cdot\mathbf{i}}) \times \\
&\qquad \frac{1}{2}(n_\beta + m_\beta e^{i\,\mathbf{Q}\cdot\mathbf{i}} + n_\beta - m_\beta e^{i\,\mathbf{Q}\cdot\mathbf{i}})], \\
&= -\frac{N}{2}(U' - \frac{J}{2})\sum_{\alpha\neq\beta} n_\alpha n_\beta + (U' - \frac{J}{2})\sum_{\mathbf{i},\alpha\neq\beta}[n_\beta(n_{\mathbf{i},\alpha,\uparrow} + n_{\mathbf{i},\alpha,\downarrow})],
\end{aligned} \tag{1.11}$$

$$
\begin{aligned}
H_3 &= -\frac{J}{2}\sum_{\mathbf{i},\alpha<\beta}[\frac{1}{2}n_{\mathbf{i},\beta,\uparrow}(n_\alpha + m_\alpha e^{i\,\mathbf{Q}\cdot\mathbf{i}}) + \frac{1}{2}n_{\mathbf{i},\alpha,\uparrow}(n_\beta + m_\beta e^{i\,\mathbf{Q}\cdot\mathbf{i}}) \\
&\quad -\frac{1}{4}(n_\alpha + m_\alpha e^{i\,\mathbf{Q}\cdot\mathbf{i}})(n_\beta + m_\beta e^{i\,\mathbf{Q}\cdot\mathbf{i}}) \\
&\quad -\frac{1}{2}n_{\mathbf{i},\beta,\uparrow}(n_\alpha - m_\alpha e^{i\,\mathbf{Q}\cdot\mathbf{i}}) - \frac{1}{2}n_{\mathbf{i},\alpha,\downarrow}(n_\beta + m_\beta e^{i\,\mathbf{Q}\cdot\mathbf{i}}) \\
&\quad +\frac{1}{2}(n_\alpha - m_\alpha e^{i\,\mathbf{Q}\cdot\mathbf{i}})(n_\beta + m_\beta e^{i\,\mathbf{Q}\cdot\mathbf{i}}) \\
&\quad -\frac{1}{2}n_{\mathbf{i},\beta,\downarrow}(n_\alpha + m_\alpha e^{i\,\mathbf{Q}\cdot\mathbf{i}}) - \frac{1}{2}n_{\mathbf{i},\alpha,\uparrow}(n_\beta - m_\beta e^{i\,\mathbf{Q}\cdot\mathbf{i}}) \\
&\quad +\frac{1}{4}(n_\alpha + m_\alpha e^{i\,\mathbf{Q}\cdot\mathbf{i}})(n_\beta - m_\beta e^{i\,\mathbf{Q}\cdot\mathbf{i}}) \\
&\quad +\frac{1}{2}n_{\mathbf{i},\beta,\downarrow}(n_\alpha - m_\alpha e^{i\,\mathbf{Q}\cdot\mathbf{i}}) + \frac{1}{2}n_{\mathbf{i},\alpha,\downarrow}(n_\beta - m_\beta e^{i\,\mathbf{Q}\cdot\mathbf{i}}) \\
&\quad -\frac{1}{4}(n_\alpha - m_\alpha e^{i\,\mathbf{Q}\cdot\mathbf{i}})(n_\beta - m_\beta e^{i\,\mathbf{Q}\cdot\mathbf{i}})] \\
&= \frac{JN}{2}\sum_{\alpha<\beta} m_\alpha m_\beta - \frac{J}{2}\sum_{\mathbf{i},\alpha\neq\beta} m_\alpha e^{i\,\mathbf{Q}\cdot\mathbf{i}}(n_{\mathbf{i},\beta,\uparrow} - n_{\mathbf{i},\beta,\downarrow}). \\
H_4 &= 0.
\end{aligned}
$$

The last term becomes zero after applying the mean-field approximation because of the Ansatz proposed.

In summary, the interaction Hamiltonian becomes:

$$
\begin{aligned}
H_{\text{int}} &= -UN\sum_\alpha \frac{1}{4}(n_\alpha^2 - m_\alpha^2) + U\sum_{\mathbf{i},\alpha}\frac{1}{2}[n_\alpha(n_{\mathbf{i},\alpha,\uparrow} + n_{\mathbf{i},\alpha,\downarrow}) \\
&\quad +m_\alpha e^{i\,\mathbf{Q}\cdot\mathbf{i}}(n_{\mathbf{i},\alpha,\downarrow} - n_{\mathbf{i},\alpha,\uparrow})] \\
&\quad -\frac{N}{2}(U' - \frac{J}{2})\sum_{\alpha\neq\beta} n_\alpha n_\beta \\
&\quad +(U' - \frac{J}{2})\sum_{\mathbf{i},\alpha\neq\beta}[n_\beta(n_{\mathbf{i},\alpha,\uparrow} + n_{\mathbf{i},\alpha,\downarrow})] \\
&\quad +\frac{JN}{2}\sum_{\alpha<\beta} m_\alpha m_\beta - \frac{J}{2}\sum_{\mathbf{i},\alpha\neq\beta} m_\alpha e^{i\,\mathbf{Q}\cdot\mathbf{i}}(n_{\mathbf{i},\beta,\uparrow} - n_{\mathbf{i},\beta,\downarrow}),
\end{aligned}
\tag{1.12}
$$

in the mean-field approximation.

1.3.4 *Fourier Transformation*

Introducing the discrete Fourier transformation as:

$$c_{\mathbf{i},\alpha,\sigma} = \frac{1}{\sqrt{N}} \sum_{\mathbf{k}} e^{i\,\mathbf{k}\cdot\mathbf{i}} c_{\mathbf{k},\alpha,\sigma}, \tag{1.13}$$

the tight-binding Hamiltonian can be transformed into momentum space via this Fourier transformation as:

$$H_{\mathrm{TB}} = \sum_{\mathbf{k},\sigma} \sum_{\alpha,\beta} \left(\xi_{\alpha\beta}(\mathbf{k}) + \epsilon_\alpha \delta_{\alpha\beta}\right) c^\dagger_{\mathbf{k},\alpha,\sigma} c_{\mathbf{k},\beta,\sigma}. \tag{1.14}$$

The interaction Hamiltonian in momentum space can be obtained by applying this Fourier transformation as:

$$\begin{aligned} H_1 &= -UN \sum_\alpha \frac{1}{4}(n_\alpha^2 - m_\alpha^2) \\ &\quad + U \sum_{\mathbf{k},\alpha} \frac{1}{2} n_\alpha (c^\dagger_{\mathbf{k},\alpha,\uparrow} c_{\mathbf{k},\alpha,\uparrow} + c^\dagger_{\mathbf{k},\alpha,\downarrow} c_{\mathbf{k},\alpha,\downarrow}) \\ &\quad - U \sum_{\mathbf{k},\alpha} \frac{1}{2} m_\alpha (c^\dagger_{\mathbf{k}+\mathbf{Q},\alpha,\uparrow} c_{\mathbf{k},\alpha,\uparrow} - c^\dagger_{\mathbf{k}+\mathbf{Q},\alpha,\downarrow} c_{\mathbf{k},\alpha,\downarrow}), \end{aligned}$$

$$\begin{aligned} H_2 &= -\frac{N}{2}(U' - \frac{J}{2}) \sum_{\alpha\neq\beta} n_\alpha n_\beta \\ &\quad + (U' - \frac{J}{2}) \sum_{\mathbf{k},\beta\neq\alpha} n_\beta (c^\dagger_{\mathbf{k},\alpha,\uparrow} c_{\mathbf{k},\alpha,\uparrow} + c^\dagger_{\mathbf{k},\alpha,\downarrow} c_{\mathbf{k},\alpha,\downarrow}), \end{aligned}$$

$$\begin{aligned} H_3 &= \frac{JN}{2} \sum_{\alpha<\beta} m_\alpha m_\beta \\ &\quad - \frac{J}{2} \sum_{\mathbf{k},\beta\neq\alpha} m_\beta (c^\dagger_{\mathbf{k}+\mathbf{Q},\alpha,\uparrow} c_{\mathbf{k},\alpha,\uparrow} - c^\dagger_{\mathbf{k}+\mathbf{Q},\alpha,\downarrow} c_{\mathbf{k},\alpha,\downarrow}). \end{aligned}$$

Therefore, the total Hamiltonian in momentum space is given by:

$$\begin{aligned} H_{\mathrm{MF}} &= H_{\mathrm{TB}} + C + \sum_{\mathbf{k},\alpha,\sigma} \epsilon_\alpha c^\dagger_{\mathbf{k},\alpha,\sigma} c_{\mathbf{k},\alpha,\sigma} \\ &\quad + \sum_{\mathbf{k},\alpha,\sigma} \eta_{\alpha,\sigma} (c^\dagger_{\mathbf{k},\alpha,\sigma} c_{\mathbf{k}+\mathbf{Q},\alpha,\sigma} + c^\dagger_{\mathbf{k}+\mathbf{Q},\alpha,\sigma} c_{\mathbf{k},\alpha,\sigma}), \end{aligned} \tag{1.15}$$

where $\mathbf{k}$ runs over the extended first Brillouin zone, H_{TB} is the hopping term in Eq. (1.14), the constant C is

$$\begin{aligned} C &= -NU \sum_\alpha \frac{1}{4} \left(n_\alpha^2 - m_\alpha^2\right) - \frac{N}{2}(2U' - J) \sum_{\alpha \neq \beta} n_\alpha n_\beta \\ &\quad + \frac{NJ}{2} \sum_{\alpha < \beta} m_\alpha m_\beta, \end{aligned} \tag{1.16}$$

N is the number of sites, and the following definitions were introduced:

$$\epsilon_\alpha = \frac{1}{2}[U n_\alpha + (2U' - J) \sum_{\beta \neq \alpha} n_\beta], \tag{1.17}$$

$$\eta_{\alpha,\sigma} = -\frac{\sigma}{2} \left(U m_\alpha + J \sum_{\beta \neq \alpha} m_\beta \right). \tag{1.18}$$

The parameters n_α and m_α can be obtained self-consistently by minimizing the energy via an iterative process. During the iterations $\sum_\alpha n_\alpha = n$ was enforced at each step, such that the total charge density is constant.

1.3.5 *Self-consistent Solving Method*

In both the Hartree-Fock approximation and the mean-field approximation, the Hamiltonian can be solved numerically by minimization of the total energy self-consistently. To illustrate this self-consistent process, let us consider the mean-field

approximation in momentum space as an example. The process in the Hartree-Fock approximation is the same as the one illustrated below. In the mean-field approximation, the Hamiltonian can be represented in matrix form in the basis:

$$\begin{aligned}\overrightarrow{c_{\mathbf{k}}} &= \{c_{\mathbf{k},1,\uparrow} \dots c_{\mathbf{k},\alpha,\uparrow}\, c_{\mathbf{k}+\mathbf{Q},1,\uparrow} \dots c_{\mathbf{k}+\mathbf{Q},\alpha,\uparrow} \\ &\qquad c_{\mathbf{k},1,\downarrow} \dots c_{\mathbf{k},\alpha,\downarrow}\, c_{\mathbf{k}+\mathbf{Q},1,\downarrow} \dots c_{\mathbf{k}+\mathbf{Q},\alpha,\downarrow}\},\end{aligned} \tag{1.19}$$

where "$1 \dots \alpha$" label the orbitals.

This Hamiltonian can be solved numerically by using standard library subroutines. The new basis where the Hamiltonian is diagonal is:

$$\overrightarrow{\gamma_{\mathbf{k}}} = \{\gamma_{\mathbf{k},1,\uparrow} \dots \gamma_{\mathbf{k},4\alpha,\uparrow}\}, \tag{1.20}$$

The relation between these two bases is:

$$\overrightarrow{c_{\mathbf{k}}} = \mathbb{V}\overrightarrow{\gamma_{\mathbf{k}}}, \tag{1.21}$$

where $\mathbb{V}$ represents eigenvectors.

From the Ansatz Eq. (1.9), we obtain:

$$n_\alpha = \frac{1}{2}\langle c^\dagger_{\mathbf{i},\alpha,\uparrow} c_{\mathbf{i},\alpha,\uparrow} + c^\dagger_{\mathbf{i},\alpha,\downarrow} c_{\mathbf{i},\alpha,\downarrow}\rangle, \tag{1.22}$$

$$m_\alpha = e^{-i\,\mathbf{Q}\cdot\mathbf{i}}\langle c^\dagger_{\mathbf{i},\alpha,\uparrow} c_{\mathbf{i},\alpha,\uparrow} - c^\dagger_{\mathbf{i},\alpha,\downarrow} c_{\mathbf{i},\alpha,\downarrow}\rangle. \tag{1.23}$$

Using Eq. (1.13), we obtain:

$$\begin{aligned} n_\alpha &= \frac{1}{2N}\langle\sum_{\mathbf{k}} e^{-i\,\mathbf{k}\cdot\mathbf{i}} c^\dagger_{\mathbf{k},\alpha,\uparrow}\sum_{\mathbf{k}'} e^{i\,\mathbf{k}'\cdot\mathbf{i}} c_{\mathbf{k}',\alpha,\uparrow} \\ &\quad + \sum_{\mathbf{k}} e^{-i\,\mathbf{k}\cdot\mathbf{i}} c^\dagger_{\mathbf{k},\alpha,\downarrow}\sum_{\mathbf{k}'} e^{i\,\mathbf{k}'\cdot\mathbf{i}} c_{\mathbf{k}',\alpha,\downarrow}\rangle, \\ m_\alpha &= \frac{1}{N} e^{-i\,\mathbf{Q}\cdot\mathbf{i}}\langle\sum_{\mathbf{k}} e^{-i\,\mathbf{k}\cdot\mathbf{i}} c^\dagger_{\mathbf{k},\alpha,\uparrow}\sum_{\mathbf{k}'} e^{i\,\mathbf{k}'\cdot\mathbf{i}} c_{\mathbf{k}',\alpha,\uparrow} \\ &\quad - \sum_{\mathbf{k}} e^{-i\,\mathbf{k}\cdot\mathbf{i}} c^\dagger_{\mathbf{k},\alpha,\downarrow}\sum_{\mathbf{k}'} e^{i\,\mathbf{k}'\cdot\mathbf{i}} c_{\mathbf{k}',\alpha,\downarrow}\rangle, \end{aligned}$$

and then plugging in the relationship Eq. (1.21), we obtain:

$$\begin{aligned} n_\alpha &= \frac{1}{2N}\sum_{\mathbf{k},\mathbf{k}'} e^{-i\,(\mathbf{k}-\mathbf{k}')\cdot\mathbf{i}}\langle\gamma^\dagger_{\mathbf{k}}(\mathbf{V}^\dagger_{\mathbf{k},\alpha,\uparrow}\mathbf{V}_{\mathbf{k}',\alpha,\uparrow} + \mathbf{V}^\dagger_{\mathbf{k},\alpha,\downarrow}\mathbf{V}_{\mathbf{k}',\alpha,\downarrow})\gamma_{\mathbf{k}'}\rangle, \\ m_\alpha &= \frac{1}{N} e^{-i\,\mathbf{Q}\cdot\mathbf{i}}\sum_{\mathbf{k},\mathbf{k}'} e^{-i\,(\mathbf{k}-\mathbf{k}')\cdot\mathbf{i}}\langle\gamma^\dagger_{\mathbf{k}}(\mathbf{V}^\dagger_{\mathbf{k},\alpha,\uparrow}\mathbf{V}_{\mathbf{k}',\alpha,\uparrow} \\ &\qquad - \mathbf{V}^\dagger_{\mathbf{k},\alpha,\downarrow}\mathbf{V}_{\mathbf{k}',\alpha,\downarrow})\gamma_{\mathbf{k}'}\rangle. \end{aligned}$$

Notice that in the ground state, we have $\langle\gamma^\dagger_{\mathbf{k}}\gamma_{\mathbf{k}'}\rangle = \delta_{\mathbf{k},\mathbf{k}'}$, then

$$\begin{aligned} n_\alpha &= \frac{1}{N}\sum_{\mathbf{k},\mathbf{k}'}\langle\gamma^\dagger_{\mathbf{k}}\mathbb{V}^\dagger\mathbb{N}_\alpha\mathbb{V}\gamma_{\mathbf{k}'}\rangle \\ &= \frac{1}{N}\sum_{\mathbf{k}\subset rBZ} Trace\{\mathbb{V}^\dagger\mathbb{N}_\alpha\mathbb{V}\}, \qquad (1.24) \\ m_\alpha &= \frac{1}{N}\sum_{\mathbf{k},\mathbf{k}'}\langle\gamma^\dagger_{\mathbf{k}}\mathbb{V}^\dagger\mathbb{M}_\alpha\mathbb{V}\gamma_{\mathbf{k}'}\rangle \\ &= \frac{1}{N}\sum_{\mathbf{k}\subset rBZ} Trace\{\mathbb{V}^\dagger\mathbb{M}_\alpha\mathbb{V}\}, \qquad (1.25) \end{aligned}$$

where we have used matrices $\mathbb{N}_\alpha$ and $\mathbb{M}_\alpha$ to represent the different products of eigenvectors for different parameters.

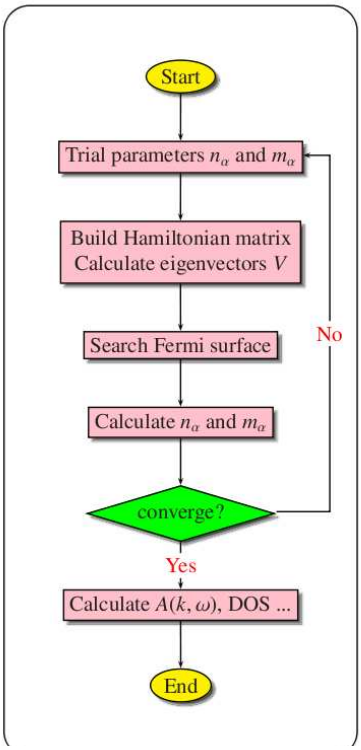

Figure 1.11: Illustration on the steps of the self-consistent solving method by solving the Hartree-Fock Hamiltonian.

With these matrices, the parameters n_α and m_α can be obtained iteratively by the following steps (Fig 1.11): (1) Choose the initial values for n_α and m_α to start with. Theoretically, the initial values can be chosen randomly, however, using an educated guess will make convergence quicker. (2) Build the Hamiltonian in a matrix form with the new n_α and m_α. Then the matrix can be diagonalized, producing all the eigenvalues and eigenvectors. (3) The Fermi surface can be obtained by searching in the eigenvalues according to the initialized chemical potential. (4) With all the information about the ground state, the new parameters n_α and m_α can be calculated. (5) Compare the old and new parameters to examine whether they are converged or not. If not, then go to *STEP* (2) to build a new Hamiltonian with the new parameters. If there is convergence, which means the correct n_α and m_α for this

system is found, then the needed physical quantities, such as the one-particle spectral function ($A(\mathbf{k},\omega)$), the DOS (density of states), the optical conductivity and Chern number can be calculated by using the mean-field eigenstates.

1.4 Optical Conductivity

1.4.1 *Theoretical Formulas*

The optical conductivity is usually denoted by $\sigma(\omega)$ and defined as:

$$\mathbf{J} = \sigma(\omega)\mathbf{E}, \tag{1.26}$$

where the electric field $\mathbf{E}$ has a time dependent magnitude

$$E = E_0 e^{i\omega t}, \tag{1.27}$$

and $\mathbf{J}$ is the induced current density. In principle, $\sigma(\omega)$ should be a second order rank tensor with nine components. However, for the pnictides we will only consider two diagonal components in the ab plane:

$$\begin{aligned} \sigma_{xx} &= J_x/E_x, \\ \sigma_{yy} &= J_y/E_y, \end{aligned} \tag{1.28}$$

and for the perovskite [111] bilayers we study the Hall conductivity:

$$\sigma_H = J_y/E_x. \tag{1.29}$$

We view this external electric field, which is uniform in space but it is time dependent, as a result of a vector potential $\mathbf{A}(\omega, t)$. The action of a particle in an electric-magnetic

field can be written as:

$$S = S_0 - e \int A^i dx_i, \tag{1.30}$$

where S_0 is the action without the field. And the phase of the wave function is proportional to the action

$$\psi \propto e^{\frac{i}{\hbar}S}, \tag{1.31}$$

so that the hopping part of the Hamiltonian becomes

$$H_{\mathrm{TB}} = \sum_{<\mathbf{i},\mathbf{l}>} \sum_{\alpha,\beta,\sigma} t_{\mathbf{il}}^{\alpha\beta} (c_{\mathbf{i},\alpha,\sigma}^{\dagger} c_{\mathbf{i+l},\beta,\sigma} e^{i\mathbf{A}(\mathbf{i},t)\cdot\mathbf{l}} + h.c.), \tag{1.32}$$

where $\mathbf{l}$ stands for the possible hopping directions $\hat{\mathbf{x}}, \hat{\mathbf{y}}, \hat{\mathbf{x}} + \hat{\mathbf{y}}, \hat{\mathbf{x}} - \hat{\mathbf{y}}$ and the units have been chosen such that $\hbar$ and electron charge e are already set to be one. The current operator and tight-binding energy operator in each direction under under the influence of an infinitesimal electric field are defined as:[57]

$$\begin{aligned} J_x &= \lim_{\mathbf{A}\to 0} -\frac{\delta H}{\delta A_x} \\ &= \sum_{<\mathbf{i},\mathbf{l}>} \sum_{\alpha,\beta,\sigma} -it_{\mathbf{il}}^{\alpha\beta} (x_{\mathbf{i}} - x_{\mathbf{i+l}}) (c_{\mathbf{i},\alpha,\sigma}^{\dagger} c_{\mathbf{i+l},\beta,\sigma} - h.c.), \\ J_y &= \lim_{\mathbf{A}\to 0} -\frac{\delta H}{\delta A_y} \\ &= \sum_{<\mathbf{i},\mathbf{l}>} \sum_{\alpha,\beta,\sigma} -it_{\mathbf{il}}^{\alpha\beta} (y_{\mathbf{i}} - y_{\mathbf{i+l}}) (c_{\mathbf{i},\alpha,\sigma}^{\dagger} c_{\mathbf{i+l},\beta,\sigma} - h.c.), \end{aligned} \tag{1.33}$$

and

$$\begin{aligned} T_x &= \sum_{<\mathbf{i},\mathbf{l}} \sum_{\alpha,\beta,\sigma} t_{\mathbf{il}}^{\alpha\beta} (x_{\mathbf{i}} - x_{\mathbf{i+l}})^2 (c_{\mathbf{i},\alpha,\sigma}^{\dagger} c_{\mathbf{i+l},\beta,\sigma} + h.c.), \\ T_y &= \sum_{<\mathbf{i},\mathbf{l}} \sum_{\alpha,\beta,\sigma} t_{\mathbf{il}}^{\alpha\beta} (y_{\mathbf{i}} - y_{\mathbf{i+l}})^2 (c_{\mathbf{i},\alpha,\sigma}^{\dagger} c_{\mathbf{i+l},\beta,\sigma} + h.c.). \end{aligned} \tag{1.34}$$

With these definitions there will be several methods to obtain the theoretical expression for $\sigma(\omega)$ and σ_H. We have used time-dependent perturbation theory, with the electric field as the perturbation, to obtain the quantum mechanical expectation value of the current and then the real part of the optical and Hall conductivity:

$$\begin{aligned} Re\sigma_{xx}(\omega) &= D_x\delta(\omega) + \frac{\pi}{A}\sum_{n\neq 0}\frac{|\langle\phi_0|J_x|\phi_n\rangle|^2}{E_n - E_0}\delta(\omega - (E_n - E_0)), \\ Re\sigma_H &= \frac{4\pi}{A}\sum_{n\neq 0} Im\frac{\langle\phi_0|J_x|\phi_n\rangle\langle\phi_n|J_y|\phi_0\rangle}{(E_n - E_0)^2}, \end{aligned} \tag{1.35}$$

and the Drude weight in the x direction D_x is given by

$$\frac{D_x}{2\pi} = \frac{\langle\phi_0| - T_x|\phi_0\rangle}{2A} - \frac{1}{A}\sum_{n\neq 0}\frac{|\langle\phi_0|J_x|\phi_n\rangle|^2}{E_n - E_0}, \tag{1.36}$$

where A is the area of the two-dimensional lattice, while ϕ_0 is the many body ground state and ϕ_n is the many body excited state, with E_0 and E_n the corresponding energies. The optical conductivity in the y direction can be obtained and expressed similarly. Due to the fact that the many body states ϕ are complicated, a direct calculation will require the number of steps in the do loop, which is the time that the optical conductivity subroutine costs, to be proportional to N^4, which limits the lattice size in our work significantly. In this sense we manually ignore all matrix elements that are identically equal to zero (for example, when there is no hopping between two states, then the corresponding element must vanish.), in order to reduce the proportional relationship to N^3 for the real space code and N for the momentum space code. After this simplification, the CPU time used on our "correlated" cluster is: six days for the 16×16 real space calculation and twenty minutes for a grid of 200×200 momentum-space points calculation.

1.4.2 *Experimental Results on Iron-Pnictides*

A variety of experiments have been performed in order to measure the optical conductivity of the pnictides. At the early stages, the behavior of the optical conductivity of different pnictides systems under different temperatures were measured by several groups[58, 59, 60, 63, 64, 61, 62, 65, 66, 67], and an example on the "122" parent compound is shown in fig 1.12.

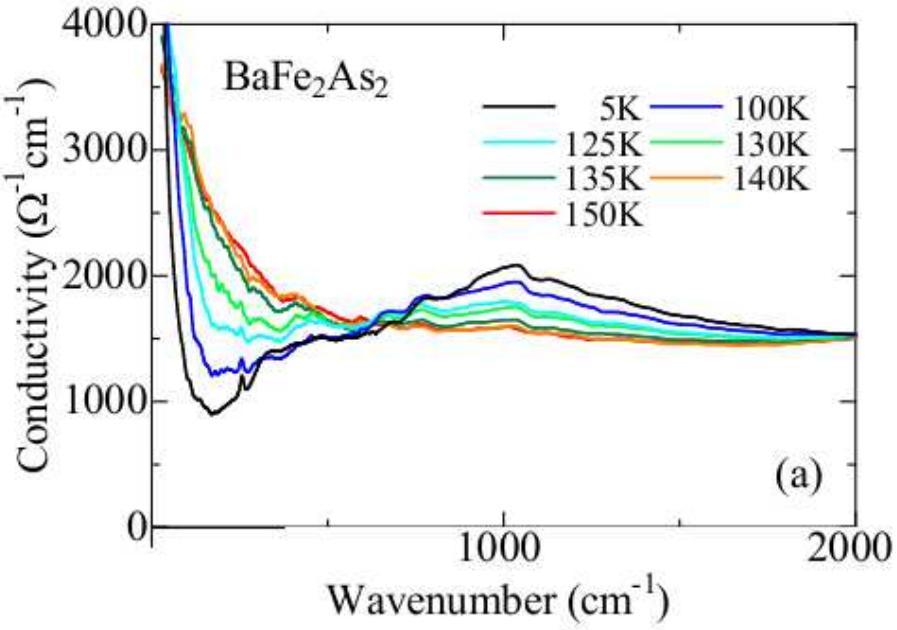

Figure 1.12: Optical conductivity spectrum of the undoped $BaFe_2As_2$ compound at several temperatures below 150 K. Reproduced from Ref [60]

A clear Drude component and another incoherent component were found[58] (Fig 1.13). This implies that there exist two electronic subsystems: one Fermi liquid subsystem and another incoherent one. It is common to determine the existence of the Fermi liquid part by the DC conductivity's $\frac{1}{T^2}$ temperature dependence, but in our project this has not been included yet. The reason is that analytically the Hartree-Fock Hamiltonian can be derived by a variational method, which gives the

lowest energy, hence requires zero temperature. Although some people do include a small temperature in order to compare with experiments, this Hartree-Fock method is not enough to follow the experiments on this point.

It is quite obvious that the electronic properties, including the optical conductivity,

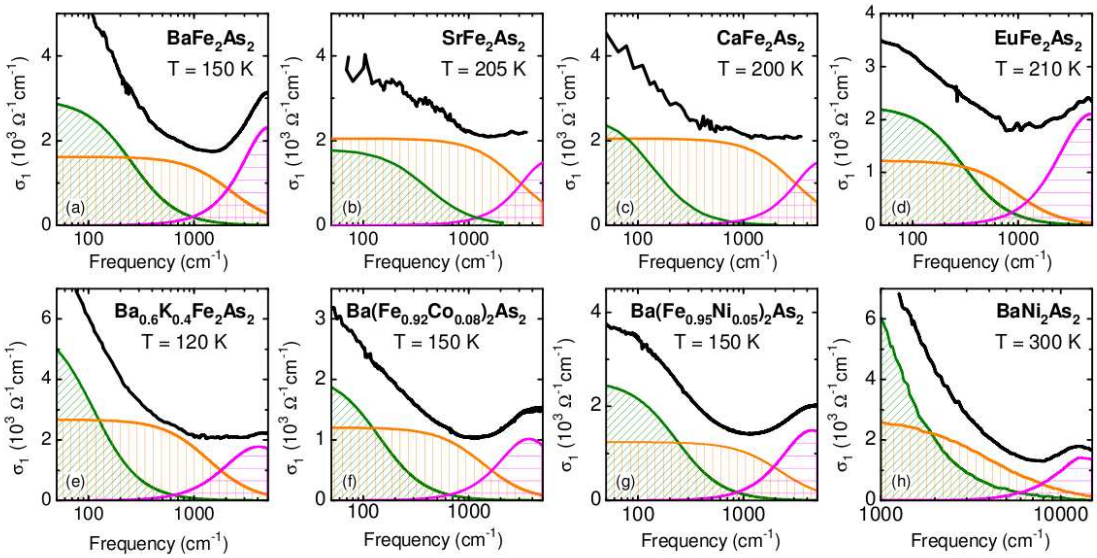

Figure 1.13: In the metallic state the optical conductivity of different iron-pnictides can always be described by two Drude terms (σ_N, green and σ_B, orange) and an oscillator in the mid-infrared (magenta). Reproduced from Ref [58].

should be anisotropic in the pnictides because the a and b directions are evidently different from each other. However, this was not observed for a long time because the samples employed in experiments used to be twinned so that the differences were averaged out. In the last year, two groups[68, 69] have discovered that, in detwinned samples, the optical conductivity shows a clear anisotropic property, and the antiferromagnetic direction has a larger optical conductivity. This is actually quite surprising at first glance because it is different from the other materials studied in the past. N. L. Wang *et al.*,[61] found that in different pnictides systems, there is a gap in the optical conductivity around $5000cm^{-1}$ (Fig 1.15), and they guessed that it may be produced by the Hund coupling and gave some intuitive illustrations in their paper.

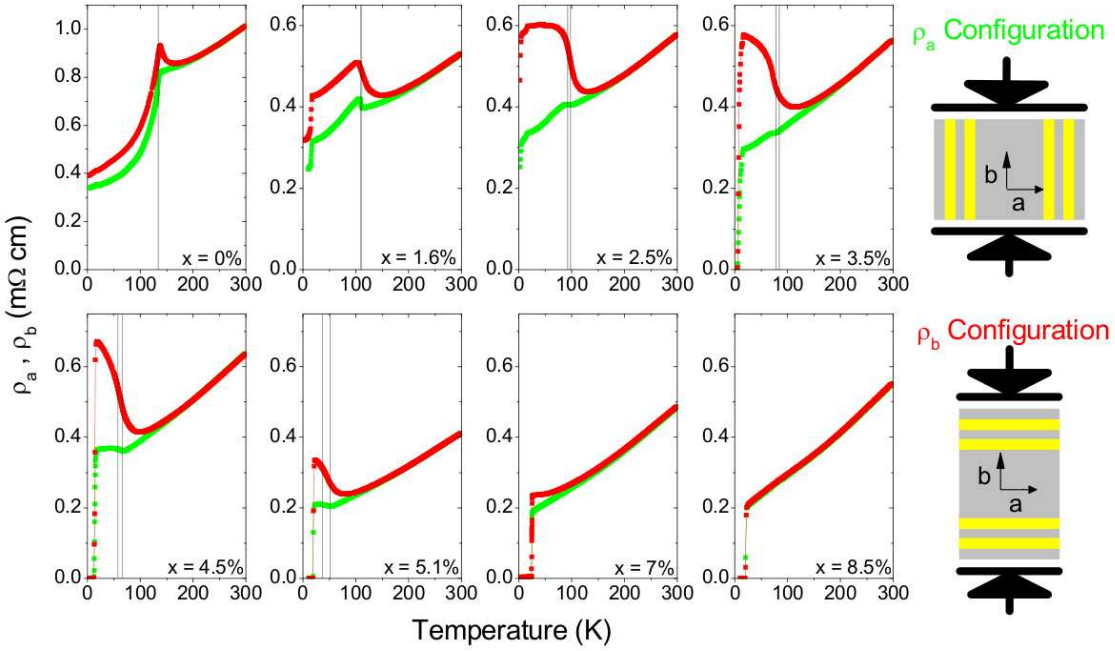

Figure 1.14: Temperature dependence of the in-plane resistivity ρ_a (green) and ρ_b (red) of $Ba(Fe_{1-x}Co_x)_2As_2$ for Co concentrations from $x = 0$ to 0.085. Solid and dashed vertical lines mark critical temperatures for the structural and magnetic phase transitions T_S and T_N respectively. Reproduced from Ref [69].

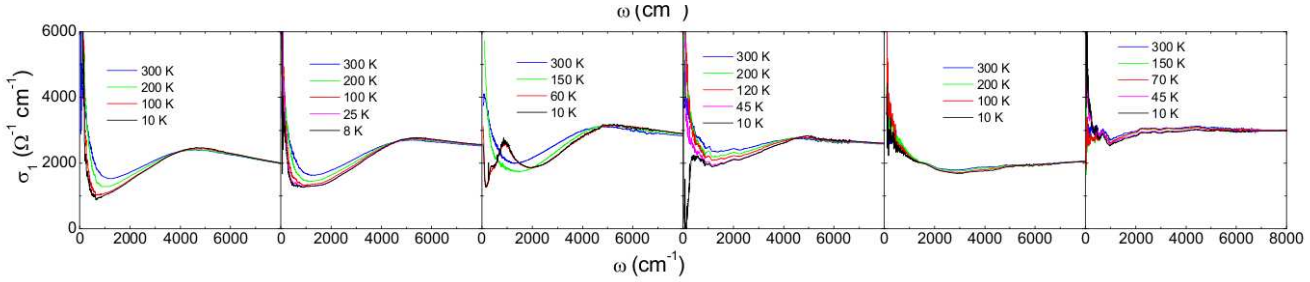

Figure 1.15: The evolution of the optical spectra of $BaFe_2As_2$ with $Co-$ and $K-$ doping. Reproduced from Ref [61]

Chapter 2

Anisotropy of the Optical Conductivity of the Iron-Pnictides from the Undoped Three-Orbital Hubbard Model

2.1 Introduction

One of the most intriguing puzzles in the study of the Fe-based high temperature superconductors [70] is the discovery of unexpected transport anisotropies in detwinned single crystals of doped and undoped AFe_2Sr_2 (A = Ba, Sr, Ca).[71] Studies of the in-plane resistivity [69] showed that the effect is the largest at low doping $x\sim$2-4% in $Ba(Fe_{1-x}Co_x)_2As_2$, but it is present even in the undoped limit x=0 at low temperatures, i.e. in the magnetically ordered state with wavevector (π,0). Recent studies [72] for the undoped 122 materials have revealed a low-temperature anisotropy (defined as $R = \rho_b/\rho_a - 1$) $R\sim$0.4, 0.35, and 0.09, for A = Ba, Sr, and Ca, respectively. This anisotropy is counter-intuitive because along the a-axis the spins order in an antiferromagnetic (AFM) arrangement, while along the b-axis they

are ferromagnetic (FM). Intuition based on, e.g., double-exchange mechanisms for manganites would suggest that the FM direction should be less resistive than the AFM one. Optical conductivity measurements concluded that this unexpected anisotropy is caused by changes in the populations of the orbitals d_{xz} and d_{yz} at the Fermi surface (FS),[73] in agreement with early mean-field studies where this unbalanced FS orbital population, without long-range orbital order, led to results compatible with photoemission techniques.[74]

Several calculations have recently addressed the experimentally observed transport anisotropy. Using a five-orbital Hubbard model treated in a mean-field approximation, and calculating the Drude weights via the Fermi velocities at the FS, results compatible with experiments were reported. [75] This agreement was observed in regimes where long-range orbital order is not present, and indeed the FS redistribution of spectral weight among the d_{xz} and d_{yz} orbitals caused by the (π,0) magnetic order[74] is needed to understand the experimental results. Other calculations also for the five-orbital Hubbard model arrived to similar conclusions.[76, 77]

In this publication, the transport anisotropy found in experiments is revisited from the perspective of a simpler three-orbital Hubbard model.[78] Our goal is to refine the intuitive explanations given in Refs. [75, 76], by focusing on the three orbitals widely believed to be the most important in pnictides, namely d_{xz}, d_{yz}, and d_{xy}, and also by identifying the electronic hopping amplitudes that cause the anisotropy. Our main results are that the experimentally observed anisotropy clearly appears in the three-orbital model, in a state that is (π,0) magnetically ordered, and it is mainly caused by the suppression of inter-hopping d_{xz}-d_{yz} processes along the FM direction.

2.2 Models and methods

In this manuscript, the three-orbital Hubbard model for the pnictides at overall electronic density n=4/3 (per site and per orbital) will be used.[78] The hopping amplitudes that reproduce the FS in the paramagnetic state, with hole and electron

$t^{\alpha\beta}_{\mathbf{il}}$	$\mathbf{l}=\mathbf{x}$	$\mathbf{l}=\mathbf{y}$	$\mathbf{l}=\mathbf{x}+\mathbf{y}$	$\mathbf{l}=\mathbf{x}-\mathbf{y}$
$\alpha\beta=11$	-0.06	-0.02	-0.03	-0.03
$\alpha\beta=22$	-0.02	-0.06	-0.03	-0.03
$\alpha\beta=33$	0.2	0.2	-0.3	-0.3
$\alpha\beta=12$	0.0	0.0	-0.01	0.01
$\alpha\beta=13$	0.2	0.0	-0.1	-0.1
$\alpha\beta=23$	0.0	0.2	-0.1	0.1

Table 2.1: Tight-binding (TB) hopping parameters of the three-orbital Hubbard model used in this manuscript. The energy unit is eV. The labeling convention is 1=d_{xz}, 2=d_{yz}, 3=d_{xy}. The 13 and 23 hoppings are all affected by a factor $(-1)^{|i|}=(-1)^{i_x+i_y}$, with $\mathbf{i}=(i_x,i_y)$ being the label of the Fe sites of a two-dimensional lattice. This modulation takes into account the two-Fe unit cell of the original FeAs layers.[78] The TB Hamiltonian is defined as $H_{\rm HT}=\sum_{\mathbf{il}\alpha\beta\sigma} t^{\alpha\beta}_{\mathbf{il}}(c^{\dagger}_{\mathbf{i},\alpha,\sigma}c_{\mathbf{i+l},\beta,\sigma}+h.c.)$, where $c^{\dagger}_{\mathbf{i},\alpha,\sigma}$ creates an electron at orbital α of site $\mathbf{i}$ with spin projection σ. $\mathbf{i}+\mathbf{l}$ denotes nearest and next-nearest neighbor sites to $\mathbf{i}$.

pockets, were already provided and discussed in detail in Ref. [78]. However, to help the readers in the understanding of our results, in Table 2.1 these intra- and inter-hopping amplitudes (in eV units) are provided again. From Table 2.1 note that the hoppings involving the d_{xy} orbital, both intra-orbital and also inter-orbital with d_{xz} and d_{yz}, are the largest in value, inducing a large Fermi velocity in the regions of the FS where the d_{xy} orbital dominates. This suggests that the d_{xy} may play an important role in the anisotropy. The Hartree mean-field approximation used here has also been much discussed in Chapter 1 and previous literature and the reader is referred to Refs. [78, 79, 80, 81] for details. The mean-field order parameters are the three electronic densities of each orbital, i.e. n_{xz}, n_{yz}, and n_{xy}, and the three magnetic moments m_{xz}, m_{yz}, and m_{xy}, and they are all determined via the minimization of the Hartree mean-field energy. In the mean-field equations, the wavevector $\mathbf{Q}=(\pi,0)$ is assumed.

Let us focus now on the optical conductivity $\sigma(\omega)$. Following well-known computational studies of $\sigma(\omega)$ in the context of the cuprates,[57] let us define first the paramagnetic current operators in the two directions as

$$\hat{j}_x = \sum_{\langle \mathbf{i},\mathbf{l}=\hat{\mathbf{x}},\hat{\mathbf{x}}+\hat{\mathbf{y}},\hat{\mathbf{x}}-\hat{\mathbf{y}}\rangle} \sum_{\alpha,\beta,\sigma} -it_{\mathbf{il}}^{\alpha\beta}(c_{\mathbf{i},\alpha,\sigma}^{\dagger} c_{\mathbf{i}+\mathbf{l},\beta,\sigma} - h.c.),$$
$$\hat{j}_y = \sum_{\langle \mathbf{i},\mathbf{l}=\hat{\mathbf{y}},\hat{\mathbf{x}}+\hat{\mathbf{y}},-\hat{\mathbf{x}}+\hat{\mathbf{y}}\rangle} \sum_{\alpha,\beta,\sigma} -it_{\mathbf{il}}^{\alpha\beta}(c_{\mathbf{i},\alpha,\sigma}^{\dagger} c_{\mathbf{i}+\mathbf{l},\beta,\sigma} - h.c.), \tag{2.1}$$

while the kinetic energy operators are

$$\hat{T}_x = \sum_{\langle \mathbf{i},\mathbf{l}=\hat{\mathbf{x}},\hat{\mathbf{x}}+\hat{\mathbf{y}},\hat{\mathbf{x}}-\hat{\mathbf{y}}\rangle} \sum_{\alpha,\beta,\sigma} t_{\mathbf{il}}^{\alpha\beta}(c_{\mathbf{i},\alpha,\sigma}^{\dagger} c_{\mathbf{i}+\mathbf{l},\beta,\sigma} + h.c.),$$
$$\hat{T}_y = \sum_{\langle \mathbf{i},\mathbf{l}=\hat{\mathbf{y}},\hat{\mathbf{x}}+\hat{\mathbf{y}},-\hat{\mathbf{x}}+\hat{\mathbf{y}}\rangle} \sum_{\alpha,\beta,\sigma} t_{\mathbf{il}}^{\alpha\beta}(c_{\mathbf{i},\alpha,\sigma}^{\dagger} c_{\mathbf{i}+\mathbf{l},\beta,\sigma} + h.c.). \tag{2.2}$$

The total current, up to the first order term in the external field $\mathbf{A}$=(A_x,A_y), can be written as $\hat{J}_x$=($\hat{j}_x + \hat{T}_x A_x$)/$N$ and $\hat{J}_y$=($\hat{j}_y + \hat{T}_y A_y$)/$N$. The real part of the optical conductivity in the x direction is given by: [57]

$$Re\sigma_{xx}(\omega) = D_x\delta(\omega) + \frac{\pi}{N}\sum_{n\neq 0}\frac{|\langle\phi_0|\hat{j}_x|\phi_n\rangle|^2}{E_n - E_0}\delta(\omega - (E_n - E_0)), \tag{2.3}$$

and from the $\sigma(\omega)$ sum-rule, it can be shown that the Drude weight in the x direction D_x is [57]

$$\frac{D_x}{2\pi} = \frac{\langle\phi_0| - \hat{T}_x|\phi_0\rangle}{2N} - \frac{1}{N}\sum_{n\neq 0}\frac{|\langle\phi_0|\hat{j}_x|\phi_n\rangle|^2}{E_n - E_0}, \tag{2.4}$$

where ϕ_0 is the many-body ground state (in this case the mean-field $\mathbf{Q}$=(π,0) state), and ϕ_n represents the many-body excited states, also produced in the mean-field calculation, with E_0 and E_n their corresponding energies. The optical conductivity and Drude weight in the y direction can be obtained and expressed similarly. N is

the number of sites. In our calculation, the Dirac δ functions are regularized as a Lorentzian $\delta(\omega)\approx(1/\pi)\epsilon/(\omega^2+\epsilon^2)$ with a small but finite broadening parameter ϵ.

2.3 Results

One of the main results found in our study is shown in Fig. 2.1 where $\sigma(\omega)$ in the two directions is shown for a state with magnetic order (π,0). The values of the couplings U and J are representative of the so-called "physical region" that was previously unveiled for the same three-orbital model.[79] In other words, by a comparison between neutron scattering and photoemission experiments against mean-field results, in previous studies it was concluded that the three-orbital model has a "physical region" (where theory matches experiments) in the range $U\sim$[0.7,1.3] and $J/U\sim$[0.15,0.33],[79] where the state is simultaneously magnetic and metallic as in pnictide parent compounds. Our $\sigma(\omega)$ study is restricted to that "physical region".

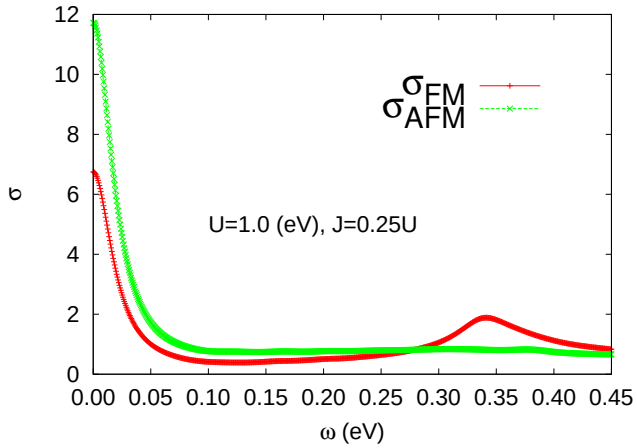

Figure 2.1: (color online) Example showing $\sigma(\omega)$ in the "physical region"[79] of the three-orbital model (ϵ=0.02). The unit of $\sigma(\omega)$ is $e^2/\hbar$. The couplings are $U=1.0$ eV and J=$U/4$. The AFM direction (i.e. the x direction for magnetic wavevector $(\pi,0)$) has a larger zero frequency conductivity than the FM direction, as in experiments. The FM direction also has a peak at a finite frequency $\sim J$.

Figure 2.1 shows that $\sigma(\omega)$ for the three-orbital model is found to be in good qualitative agreement with experiments, namely at small frequency ω, where the

Drude peak is located, the weight of this peak is larger along the AFM direction (the x direction) than along the FM direction. Similar results were obtained in the entire "physical region", see Fig. 2.2. In addition, the finite frequency peak in the FM direction was found to scale with J. The ratio $D_{\rm AFM}/D_{\rm FM}$ (i.e. D_x/D_y) in the range of U shown in Fig. 2.2 varies approximately between 1.6 and 2.2, in qualitative agreement with results for the five-orbital model.[75, 76] Thus, it is here concluded that the three-orbital model [78] is sufficient to reproduce the d.c. conductivity anisotropy found in experiments. [71]

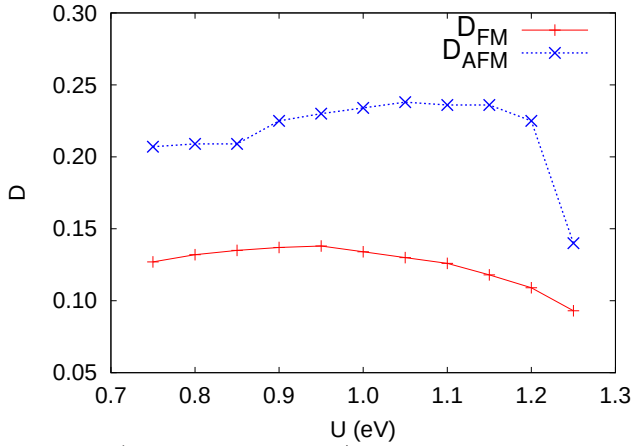

Figure 2.2: (color online) Drude weight/π *vs.* U in the "physical region" of the three-orbital model, at J=U/4. In this regime, the inequality $D_{\rm AFM}$>$D_{\rm FM}$ holds. As U increases toward the upper limit shown, the Drude weights in both directions are reduced due to increasing insulating tendencies.[79]

For completeness, in Fig. 2.3(a) the population of the three orbitals is shown in the range of U's studied. From this figure, it is clear that there is no orbital order since the orbitals d_{xz} and d_{yz} are nearly identically populated. Further increasing U eventually leads to a regime of orbital-order,[78] but the opening of a gap renders the system insulating. It is important to note that Fig. 2.3(a) contains results obtained by integrating the orbital-selective density-of-states over all frequencies, while if the focus is only the vicinity of the FS, the orbital-weight redistribution phenomenon is observed.[78] As shown below, this redistribution is important to understand the anisotropy.

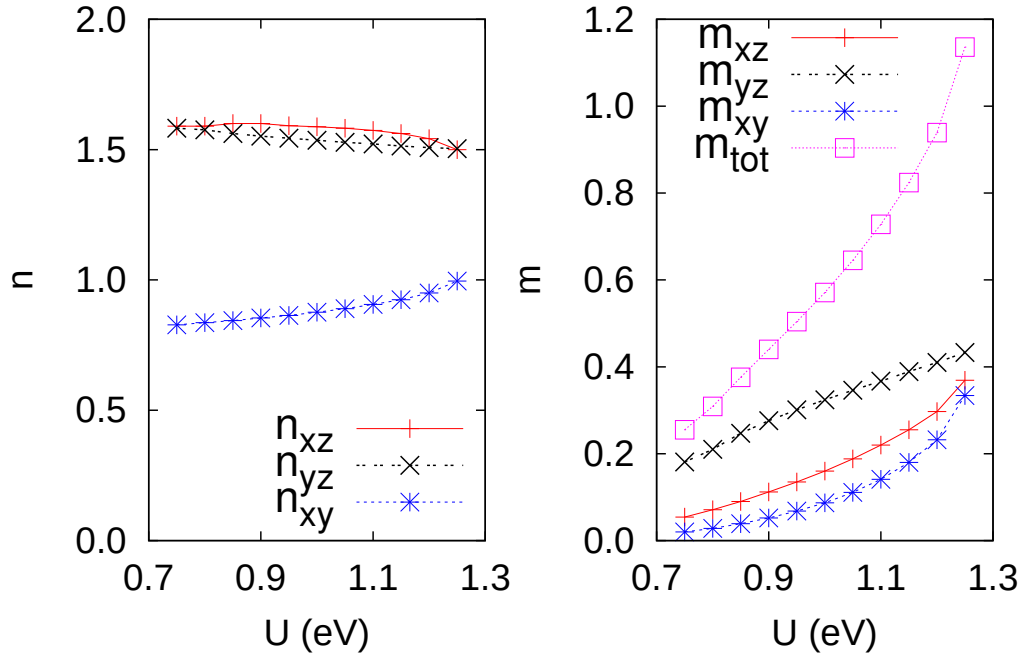

Figure 2.3: (color online) (a) Charge density of each orbital *vs.* U in the "physical region" of the three-orbital model, at J=$U/4$, and for spin order $(\pi, 0)$. (b) m_α *vs.* U in the same U range, at J=$U/4$, and for spin order $(\pi, 0)$.

In addition, Fig. 2.3(b) shows that the magnetic moment in the range investigated is compatible with pnictides neutron experiments, ranging from ∼0.25 Bohr magnetons (μ_B) for the 1111 to ∼1 μ_B for the 122 compounds.[79]

2.4 Intuitive origin of the anisotropy

While the notion of an orbital weight redistribution at the FS is well established,[74, 75] with the d_{yz} orbital suppressed for $\mathbf{Q}$=(π,0), it is desirable to develop a more intuitive understanding of its influence on transport properties. For this purpose, the kinetic energy and current operators will be expressed in momentum space as:

$$\hat{T}_a = \sum_{\mathbf{k}} \sum_{\alpha,\beta,\sigma} t_a^{\alpha\beta}(\mathbf{k}) c^{\dagger}_{\mathbf{k},\alpha,\sigma} c_{\mathbf{k},\beta,\sigma} = \sum_{\mathbf{k}} \hat{T}_a(\mathbf{k}),$$
$$\hat{j}_a = \sum_{\mathbf{k}} \sum_{\alpha,\beta,\sigma} j_a^{\alpha\beta}(\mathbf{k}) c^{\dagger}_{\mathbf{k},\alpha,\sigma} c_{\mathbf{k},\beta,\sigma} = \sum_{\mathbf{k}} \hat{j}_a(\mathbf{k}), \tag{2.5}$$

where a is the direction index (x, y). From Eq.(4), the $\mathbf{k}$ contribution (unfolded first Brillouin zone) to the Drude weight is defined as $D_a(\mathbf{k})$=$D_{1,a}(\mathbf{k})$-$D_{2,a}(\mathbf{k})$, where

$$\frac{D_{1,a}(\mathbf{k})}{2\pi} = \frac{\langle\phi_0| - \hat{T}_a(\mathbf{k})|\phi_0\rangle}{2N},$$
$$\frac{D_{2,a}(\mathbf{k})}{2\pi} = \frac{1}{N}\sum_{n\neq 0} Re\frac{\langle\phi_0|\hat{j}_a(\mathbf{k})|\phi_n\rangle \times \langle\phi_n|\hat{j}_a|\phi_0\rangle}{E_n - E_0}, \tag{2.6}$$

since summing over $\mathbf{k}$ leads to Eq. (4).

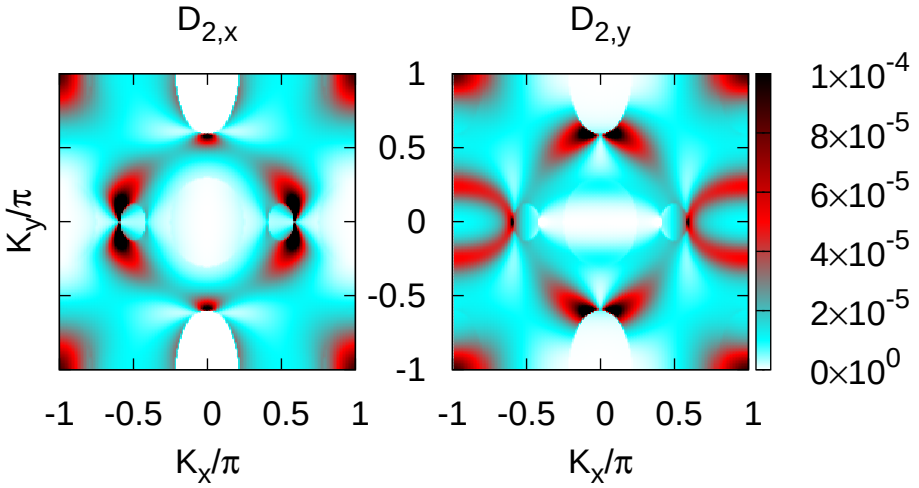

Figure 2.4: (color online) $D_{2,a}(\mathbf{k})/\pi$ in the "physical region"[79] of the three-orbital model (U=1.0 eV, J=$U/4$) and with spin order $(\pi, 0)$. For a discussion of the results see text.

From Fig. 2.4 (right panel) it is clear that the $(\pi, 0)$ pocket contributes significantly to $D_{2,y}$ since this wavevector region has sizable intensity. However, the contribution of the $(0, \pi)$ pocket to $D_{2,x}$ is negligible, thus inducing the significant anisotropy observed in the overall Drude weight (note that the rest of the highly intense features in $D_{2,y}$ are $\pi/2$-rotated those of $D_{2,x}$ and thus do not contribute to the anisotropy). The reason is the orbital weight redistribution at the FS: according to nesting scenarios, the $(0, 0)$ pocket (with mainly d_{xz} and d_{yz} character), interacts with the $(\pi, 0)$ pocket (mainly d_{xy} and d_{yz}) when the magnetic wavevector is $\mathbf{Q}$=(π,0). This interaction needs to be intra-orbital,[82] hence the d_{yz} states at the $(\pi, 0)$ pocket are raised above the FS, while the d_{xy} states are not. On the other hand, the $(0, \pi)$ states are not moved above the FS if $\mathbf{Q}$=(π,0), and hence this phenomenon does not occur for $D_{2,x}$. Note that the results of Fig. 2.4 based on the Drude weights directly address the anisotropy in transport, and complements the analysis based on the orbital-weight redistribution.[74, 75] Also note that a similar analysis of $D_{1,y}$ and $D_{1,x}$ (not shown) does not lead to the same clear anisotropy that $D_{2,a}$ provides.

To further simplify the understanding of the anisotropy evident in Fig. 2.4 let us now focus on the most relevant electronic hopping processes. Analyzing the values of the hopping amplitudes (Table 1), it is clear that those involving the d_{xy} orbital (both inter- and intra-orbital) should be the most relevant since the other hoppings are much smaller in magnitude. The direct intra-orbital hopping d_{xy}-d_{xy} ($t_{\mathbf{il}}^{33}$ in Table 1) is not suppressed at the FS and should equally contribute to charge transport in both directions. Thus, the conductance should not drop to zero in any of the two directions due to this intra-orbital contribution. However, the inter-orbital hopping d_{xy}-d_{yz} is suppressed at the FS in a magnetic state (π,0). This hopping occurs *only* along the y direction, as previously discussed.[78] On the other hand, the hopping d_{xy}-d_{xz} is *not* suppressed and can contribute to electronic hopping along the x direction. For these reasons, an asymmetry is expected between the x and y directions in transport, as found in Fig. 2.1. In addition, for $\mathbf{k}$ close to the $(\pi, 0)$ pocket the inter-orbital d_{xy}-d_{yz} hopping, which only exists along the y direction, needs an excitation to contribute

to $\sigma(\omega)$ along the FM direction (y-axis) because d_{yz} is suppressed at the FS. This observation justifies the presence of a peak scaling with J in $\sigma_{\rm FM}$ (Fig. 1).

To transform the intuition developed above based on hopping amplitudes into actual transport properties, the Drude weight will also be decomposed according to the hoppings corresponding to the different orbitals, via the following definitions:

$$\frac{D_a^{\alpha\beta}}{2\pi} = -\frac{\langle\phi_0|\hat{T}_a^{\alpha\beta}+\hat{T}_a^{\beta\alpha}|\phi_0\rangle}{2N} - \frac{1}{N}\sum_{n\neq 0} Re\frac{\langle\phi_0|\hat{j}_a^{\alpha\beta}+\hat{j}_a^{\beta\alpha}|\phi_n\rangle\langle\phi_n|\hat{j}_a|\phi_0\rangle}{E_n-E_0}, \qquad (2.7)$$

for inter-orbital hopping ($\alpha\neq\beta$) (a=x,y). The operators in Eq. (7) arise from Eq. (2) via $\hat{T}_a$=$\sum_{a,\alpha\beta}\hat{T}_a^{\alpha\beta}$ and $\hat{j}_a$=$\sum_{a,\alpha\beta}\hat{j}_a^{\alpha\beta}$. For the case of intra-orbital, the diagonal Drude weight $D_a^{\alpha\alpha}$ is obtained from Eq. (7) by replacing $\hat{T}_a^{\alpha\beta}$+$\hat{T}_a^{\beta\alpha}$ by $\hat{T}_a^{\alpha\alpha}$ and $\hat{j}_a^{\alpha\beta}$+$\hat{j}_a^{\beta\alpha}$ by $\hat{j}_a^{\alpha\alpha}$. The several Drude components obtained by this procedure are in Table 2.2. From this Table, it can be seen that the main anisotropy arises from the fact that D_x^{13}∼0.125 is an order of magnitude larger than D_y^{23}∼0.011, due to the FS suppression of the d_{yz} orbital. The rest of the contributions in Table 2.2 that are unrelated to the inter-orbital hopping involving d_{xy} are similar in both directions and are not relevant to understand the anisotropy. Actually, for the largest of those, the naive intuition suggesting a better conductance along the FM direction *is* satisfied since D_y^{33}>D_x^{33}.

2.5 Summary.

A mean-field study of $\sigma(\omega)$ employing a three-orbital Hubbard model for the magnetically ordered parent compounds of the pnictides has been here reported. In agreement with experiments, the conductance along the AFM direction is shown to be larger than along the FM direction. The simplicity of this model allowed us to reduce this effect to an intuitive picture: (i) The AFM conductance behaves normally with a notorious suppression of its value as compared with the non-interacting limit due to spin scattering, in agreement with intuition. (ii) However, along the FM

$\alpha\beta$	11	22	33	12	13	23
$D_x^{\alpha\beta}$	0.019	-0.003	0.073	0.013	0.125	0.005
$D_y^{\alpha\beta}$	0.020	0.002	0.087	0.014	-0.01	0.011

Table 2.2: Drude weight/π decomposed into the different orbitals (1=d_{xz}, 2=d_{yz}, 3=d_{xy}) of the three-orbital model working at U=1.0 eV and J=0.25U. Finding negative Drude weights in some cases is a well-known effect[57] arising from differences of two large numbers in Eq. (4).

direction the drastic reduction in the weight of the d_{yz} orbital at the FS leads to a large effective *suppression* of the d_{xy}-d_{yz} hopping and associated conductance along that FM direction, using the anisotropy found experimentally.

Chapter 3

Study on Flat Band Physics in Perovskite [111] Bilayers by Two-Orbital Hubbard Model

3.1 Introduction

In recent years, it has been made increasingly clear that the band topology of crystals can have a profound effect on material properties. One of the examples is the celebrated quantum Hall effect (QHE), in which the quantized Hall conductance can be expressed as a topological number of the magnetic Bloch bands. However, it was long believed that such topological states are rather exotic and are restricted to low temperatures, reduced dimensionality and high magnetic field. This view was changed when Haldane first proposed that electrons hopping on a honeycomb lattice could realize the QHE in the absence of Landau levels, pointing out the possibility of non-trivial topology in simple band insulators.[46] Along this direction, recent efforts have culminated in the theoretical prediction[47, 48, 49, 50] and subsequent experimental realization[51, 52, 53, 54, 55] of the so-called topological insulators (TIs). In these materials, the strong spin-orbit coupling (SOC) plays the role of magnetic field in the

QHE and leads to the emergence of nontrivial band topology. So far, the existence of TIs has been experimentally demonstrated in several classes of materials, including HgTe quantum well,[51] $Bi_{1-x}Sb_x$ alloy,[52] and tetradymite semiconductors such as Bi_2Se_3,[53] Bi_2Te_3,[54] and Sb_2Te_3.[55]

After the initial discovery of TIs, the current research is now focused on the interplay between nontrivial band topology and electron correlations. For this purpose, transition metal oxides (TMO), particularly $4d$ and $5d$-electron compounds, provide a natural material platform. First of all, in heavy transition metal atoms the SOC can be large, which is essential to realize topological phases. Secondly, electrons in such materials are usually strongly correlated and hence many body physics is important. Recently, it was predicted that bilayers of perovskite-type transition-metal oxides grown along the [111] crystallographic axis are potential candidates for two-dimensional topological insulators.[56] The topological band structure of these materials can be fine-tuned by changing dopant ions, substrates and external gate voltages. The most striking feature of these materials is probably the existence of nearly flat topological bands in e_g systems. When such bands are partially filled, kinetic energy is suppressed and the physics is controlled mainly by interaction, which may produce new and interesting phases. One possibility is the emergence of the fractional quantum Hall liquids in the absence of an external magnetic field. This has been the subject of several recent works. In this chapter, we shall explore another interesting scenario, *i.e.*, when the flat bands is half filled, what is the ground state? And how does doping change the phase?

3.2 Model and Method

Here we apply a two-orbital Hubbard model and spin-orbital coupling for the two e_g orbitals. In this work, all quantities with the dimension of energy are in the unit of t_σ of the e_g electrons. The tight-binding part of the Hamiltonian can be found in

Ref. [56] and the interaction part reads:

$$\begin{aligned} H_{\text{int}} &= U\sum_{\mathbf{i},a,\alpha} n_{\mathbf{i},a,\alpha,\uparrow} n_{\mathbf{i},a,\alpha,\downarrow} \\ &+(U'-\frac{J}{2})\sum_{\mathbf{i},a,\alpha<\beta} n_{\mathbf{i},a,\alpha} n_{\mathbf{i},a,\beta} \\ &-2J\sum_{\mathbf{i},a,\alpha<\beta} \mathbf{S}_{\mathbf{i},a,\alpha}\cdot\mathbf{S}_{\mathbf{i},a,\beta} \\ &+J\sum_{\mathbf{i},a,\alpha<\beta} (c^{\dagger}_{\mathbf{i},a,\alpha,\uparrow} c^{\dagger}_{\mathbf{i},a,\alpha,\downarrow} c_{\mathbf{i},a,\beta,\downarrow} c_{\mathbf{i},a,\beta,\uparrow} + h.c.), \end{aligned} \tag{3.1}$$

where $\mathbf{S}_{\mathbf{i},a,\alpha}$ ($n_{\mathbf{i},a,\alpha}$) is the spin (charge density) of orbital α at site $\mathbf{i}$ and sublattice a, and $n_{\mathbf{i},a,\alpha} = n_{\mathbf{i},a,\alpha,\uparrow} + n_{\mathbf{i},a,\alpha,\downarrow}$. The on-site interaction parameters include the inter-orbital repulsion U, the intra-orbital repulsion $U^{'}$ and the Hund coupling J with the constraint $U^{'} = U - 2J$. In this work, we fix the ratio J/U to be 0.25 just for convenience. The spin-orbital coupling part of the Hamiltonian is written as:

$$H_{\text{SOC}} = -\frac{\lambda}{2}\sum_{\mathbf{i},a} \tau_{y,\mathbf{i},a}\otimes\sigma_{z,\mathbf{i},a}, \tag{3.2}$$

where τ_y is the pseudo spin operator in the orbital space and σ_z is the Pauli matrix in the spin space. Here the z axis is chosen to be along the [111] direction.This Hamiltonian is solved by minimizing the Hartree-Fock mean-field energy via an iteration process. The lattice size is chosen to be 8×8. Here, in the honeycomb lattice, by 8×8 we mean that the lattice has 64 transition metal atoms and one can find 8 of them by going along both the zigzag (X direction in Fig 1.8 c) and the armchair (Y direction in Fig 1.8 c) sides. The periodic boundary conditions are applied.

Now let us consider the Hall conductance of the system, which can be calculated according to the Kubo formula as:[57]

$$\sigma_H = \frac{4\pi}{A}\sum_{n\neq 0} Im\frac{\langle\phi_0|\hat{j}_x|\phi_n\rangle\langle\phi_n|\hat{j}_y|\phi_0\rangle}{(E_n-E_0)^2}, \tag{3.3}$$

where ϕ_0 is the many-body ground state and ϕ_n represents the many-body excited states, with E_0 and E_n their corresponding energies. A is the area of the lattice. $\hat{j}_x$ and $\hat{j}_y$ are the paramagnetic current operators in the two directions with the definition:

$$\begin{aligned}\hat{j}_x &= \sum_{\langle \mathbf{i},a,\mathbf{l},a'\rangle} \sum_{\alpha,\beta,\sigma} it^{\alpha\beta}_{\mathbf{i},a,\mathbf{l},a'}(x_{\mathbf{i},a} - x_{\mathbf{i}+\mathbf{l},a'})(c^{\dagger}_{\mathbf{i},a,\alpha,\sigma}c_{\mathbf{i}+\mathbf{l},a',\beta,\sigma} - h.c.), \\ \hat{j}_y &= \sum_{\langle \mathbf{i},a,\mathbf{l},a'\rangle} \sum_{\alpha,\beta,\sigma} it^{\alpha\beta}_{\mathbf{i},a,\mathbf{l},a'}(y_{\mathbf{i},a} - y_{\mathbf{i}+\mathbf{l},a'})(c^{\dagger}_{\mathbf{i},a,\alpha,\sigma}c_{\mathbf{i}+\mathbf{l},a',\beta,\sigma} - h.c.).\end{aligned} \tag{3.4}$$

3.3 Results

Here we first investigate the undoped case when the electron number per site is $n = 0.5$ and hence the flat band is half-filled. The magnetic order parameter is defined as:

$$\begin{aligned} m =& \sum_{\alpha} m_{\alpha} \\ =& \frac{2}{N} \sum_{\mathbf{i}\alpha} \sqrt{\langle \sigma_{\mathbf{i}x}\rangle^2 + \langle \sigma_{\mathbf{i}y}\rangle^2 + \langle \sigma_{\mathbf{i}z}\rangle^2}, \end{aligned} \tag{3.5}$$

where N is the number of atoms. We choose to normalize the maximum value of m at $n = 0.5$ to be 1. The phase diagram shown in Fig. 3.1 is obtained. We can see that there is a second order phase transition (except for λ exactly equal to zero, where it is first order) from a non-magnetic, 0 Hall conductance phase to a magnetic one with Hall conductance equals to ± 1 in the unit of e^2/h when we increase the value of U. The required U for the transition to occur increases with λ. The charge and spin configuration in this phase is plotted in Fig. 3.2, which clearly shows that the charge is uniformly distributed and the whole system is ferromagnetic.

This effect was predicted to occur under a Zeeman field in Ref. [56] but now we realize it by the Coulomb interaction between electrons. Here we discuss the connection between the two approaches. From the real space calculation we see that in the magnetic phase all spins are polarized into a common direction. This is due to the electron-electron interaction that splits each band into two sub-bands with

different spin. For simplicity but without losing generality, from now on let us say that the spin-up sub-band is below the spin-down one. Hence we insert the Hartree Ansatz

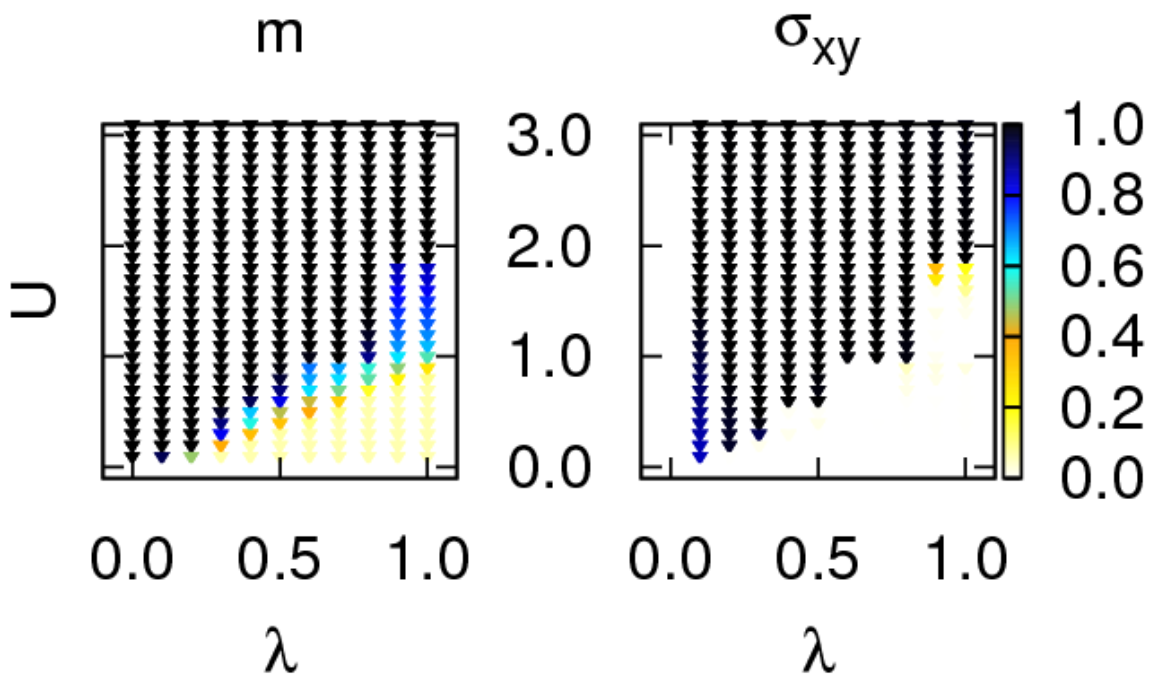

Figure 3.1: Order parameter m (left panel) and Hall conductance σ_H (right panel) vs U and λ, when $n = 0.5$. From this figure, we observe that the system is ferromagnetic with all spins pointing upward in a large portion of the phase diagram.

$$\langle c^{\dagger}_{\mathbf{i},a,\alpha,\sigma} c_{\mathbf{i}',a',\alpha',\sigma'} \rangle = (\frac{1}{2} n_\alpha + \frac{\sigma}{2} m_\alpha) \delta_{\mathbf{i}\mathbf{i}'} \delta_{aa'} \delta_{\alpha\alpha'} \delta_{\sigma\sigma'}, \tag{3.6}$$

which describes the uniform ferromagnetic order, and transform it into momentum space. The interaction Hamiltonian in momentum space is found to be

$$H_{\text{int}} = C + \sum_{\mathbf{k},a,\alpha,\sigma} (\epsilon_\alpha + \eta_{\alpha,\sigma}) c^{\dagger}_{\mathbf{k},a,\alpha,\sigma} c_{\mathbf{k},a,\alpha,\sigma}, \tag{3.7}$$

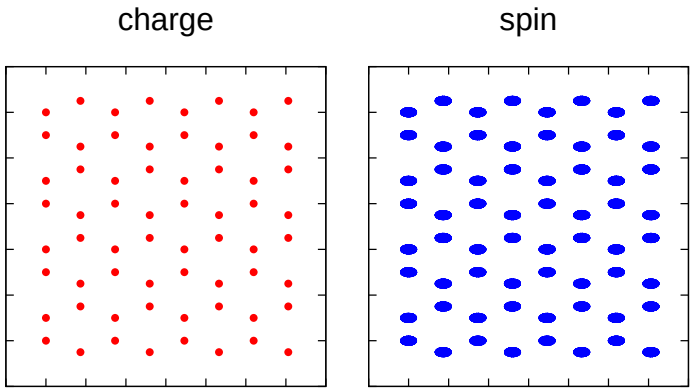

Figure 3.2: Charge (left panel) and spin (right panel) configurations when m is maximized for the case $n = 0.5$.

where the following definitions are introduced:

$$\begin{aligned} C &= -\frac{NU}{4}\sum_{\alpha}\left(n_{\alpha}^{2}-m_{\alpha}^{2}\right)-N(2U'-J)\sum_{\alpha\neq\beta}\frac{1}{4}n_{\alpha}n_{\beta} \\ &\quad +\frac{NJ}{2}\sum_{\alpha<\beta}m_{\alpha}m_{\beta}, \\ \epsilon_{\alpha} &= \frac{U}{2}n_{\alpha}+(U'-\frac{J}{2})\sum_{\beta\neq\alpha}n_{\beta}, \\ \eta_{\alpha,\sigma} &= -\frac{\sigma}{2}\left(Um_{\alpha}+J\sum_{\beta\neq\alpha}m_{\beta}\right). \end{aligned} \tag{3.8}$$

Now it is clear that what causes the Zeeman splitting is $\eta_{\alpha,\sigma}$ and the corresponding energy is

$$E_{Zeeman} = -S_z\left(Um_{\alpha}+J\sum_{\beta\neq\alpha}m_{\beta}\right), \tag{3.9}$$

so that the effective magnetic field is

$$B_{eff} = \frac{-1}{g_s \mu_B} \left(U m_\alpha + J \sum_{\beta \neq \alpha} m_\beta \right), \tag{3.10}$$

where g_s is the Landé factor and μ_B is the Bohr magneton.

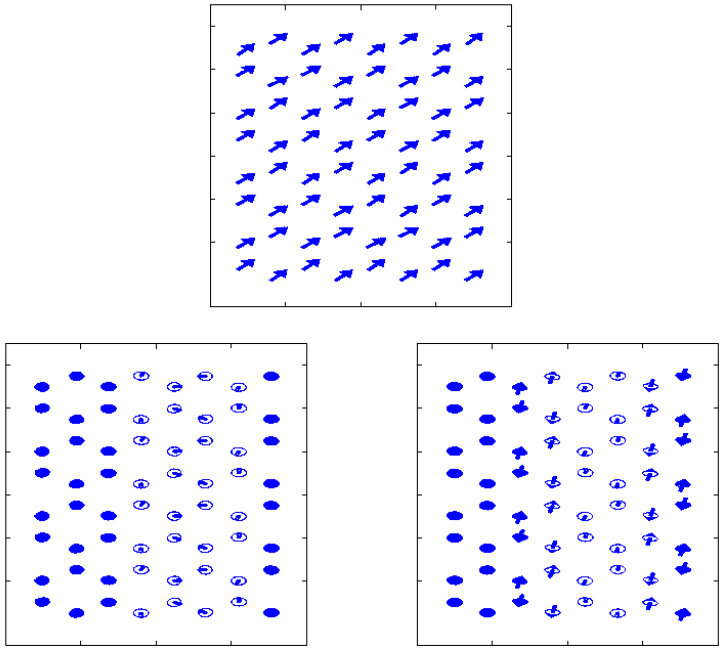

Figure 3.3: Spin configurations at $U = 0.5$, $\lambda = 1.0$ (up panel) and $U = 1.1$, $\lambda = 1.0$, $3z^2 - r^2$ orbital (left panel), $x^2 - y^2$ orbital (right panel), when $n = 0.5$.

From Fig. 3.1 we clearly see that the Hall conductance does not appear until the order parameter m almost reaches its maximum value. Let us also discuss what happens during this second order transition when the order parameter m is non-zero but it is also not maximized. From a Bloch band point of view, the existence of this regime is due to the band dispersion induced by λ. When the band is not completely flat, the top of the spin-up sub-band is higher than the bottom of the spin-down sub-band if U and J are non-zero but also not large enough. In this case, electrons with both kinds of spin exist together and the number of spin-down electrons should

gradually vanish with increasing U. The configurations in this regime are shown in Fig. 3.3. At relatively low value of U/λ, the order parameter m is still very small and the whole system is ferromagnetic. As we increase the value of U/λ so that spin-up and spin-down electrons prefer to be separated from each other but the number of spin-down electrons is still large, the system includes two almost ferromagnetic domains with spin almost up and down. In this regime, electrons in the two e_g orbitals have different spin orientations. Especially on the domain walls, the orientations are quite different. If we still increase the value of U/λ, the number of spin-down electrons will decrease to zero and the system gradually comes to a ferromagnetic state. Of course, the value $\lambda = 1.0$ as used in Fig. 3.3 is too large to be realistic. However, because this domain configuration is due to the band being no longer completely flat when λ is present, it only exist in a considerable U range when λ is large. For small λ values, this configuration is also found, but only in a very small range of U. For example, at $\lambda = 0.3$ the U region that gives this domain pattern has a width about 0.04, while at $\lambda = 1.0$ this width ~ 1. For this reason, we choose $\lambda = 1.0$ to show more clear information.

Now let us move a little bit alway from $n = 0.5$ by doping 4 electrons into the lattice with 64 transition metal atoms so that $n = 0.5625$. In this case, unless U is very large, the doped 4 electrons are more likely to be spin-down and hence intuitively they will strengthen the domain configuration in the transition regime discussed above. However, calculations show more interesting results. In the domain case at $n = 0.5$, the charge density is uniform in real space. In this doped case, we find that the sites on the domain walls have higher charge density and local density of states (LDOS) at the Fermi energy, as shown in Fig. 3.4. This means the physics is different from the undoped case. Now the system has two regions with Chern number ± 1 and a topological edge-state appears at the boundary. It is evident that this edge-state should be conducting, but at a first glance it seems that the ferromagnetic domains are also conducting because the LDOS(E_F) there does not vanish. However, remember that in Fig. 3.4 U is chosen to be 1.1, which is the same as in the two

lower panels of Fig. 3.3 and still in the transition area at $n = 0.5$ (Fig. 3.1). When we enlarge U to 3.0, which is able to produce the uniform, ferromagnetic phase in the undoped case, we see the result shown in Fig. 3.5. The doped charge density and LDOS(E_F) almost vanish inside the magnetic domains. Hole doping gives almost the same result.

3.4 Summary

We have studied the roll of electron-electron interactions in the flat band physics of perovskite [111] bilayers. We found that this on-site Coulomb interaction will lead to a spontaneous symmetry breaking in the spin space which introduces a transition from a band insulator into a Chern-insulator. When the spin-orbital coupling λ is present, the band is no longer absolutely flat so that the transition is second order. In this case, another case of spontaneous symmetry breaking, this time in real space, is obtained. It induces on-site magnetic moments in the system and causes the domain configurations. As the strength of the Coulomb interaction increases, one spin direction dominates over the other and finally the system becomes a quantum Hall ferromagnet. When small amount of electrons or holes are doped into this domain pattern, the doped particles are more likely to concentrate on the domain walls and form an edge-state.

One kind of famous and well-studied perovskite-structure materials with active e_g electrons is the manganites family. In the bulk limit, some of them are found to be ferromagnetic at $n = 0.5$ experimentally[83] and numerical calculations based on double-exchange model also showed that when Heisenberg coupling is weak enough the ground state is ferromagnetic[84]. It is possible that in the [111] bilayer of the manganites at $n = 0.5$ the ferromagnetic phase also exist, then manganites can be a potential family of materials in which the phenomena discussed in this paper can be realized.

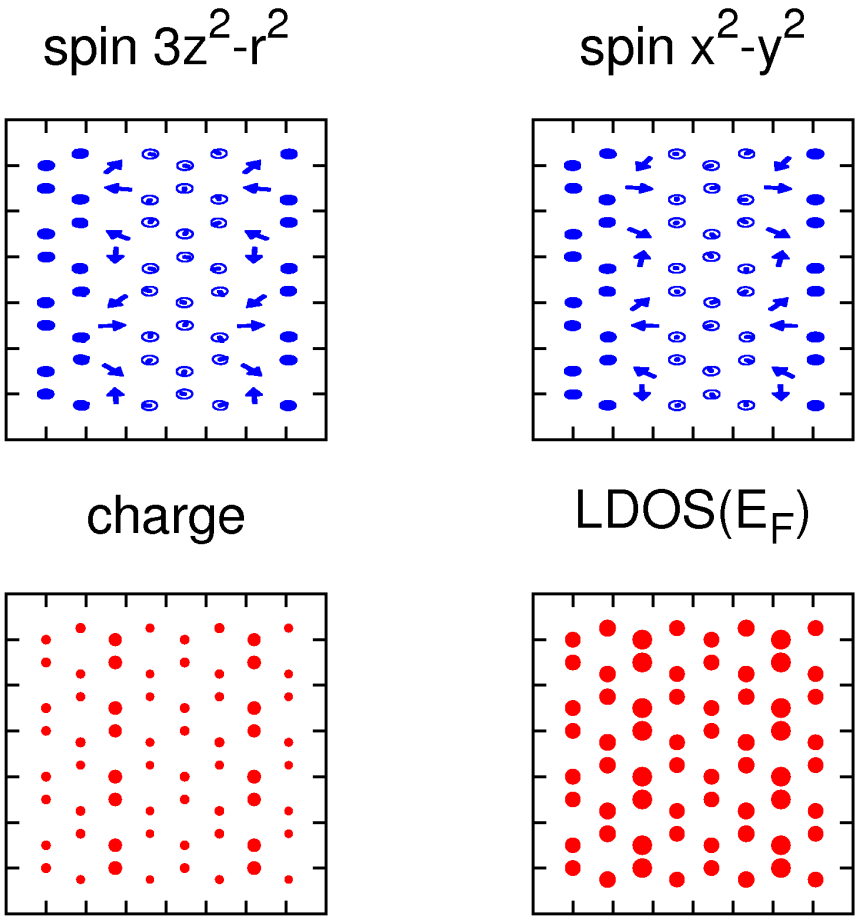

Figure 3.4: Spin in the $3z^2 - r^2$ orbital (upper left panel), the $x^2 - y^2$ orbital (upper right panel), doped charge (lower left panel) and LDOS(E_F) (lower right panel) at $U = 1.1$, $\lambda = 1.0$ when $n = 0.5625$.

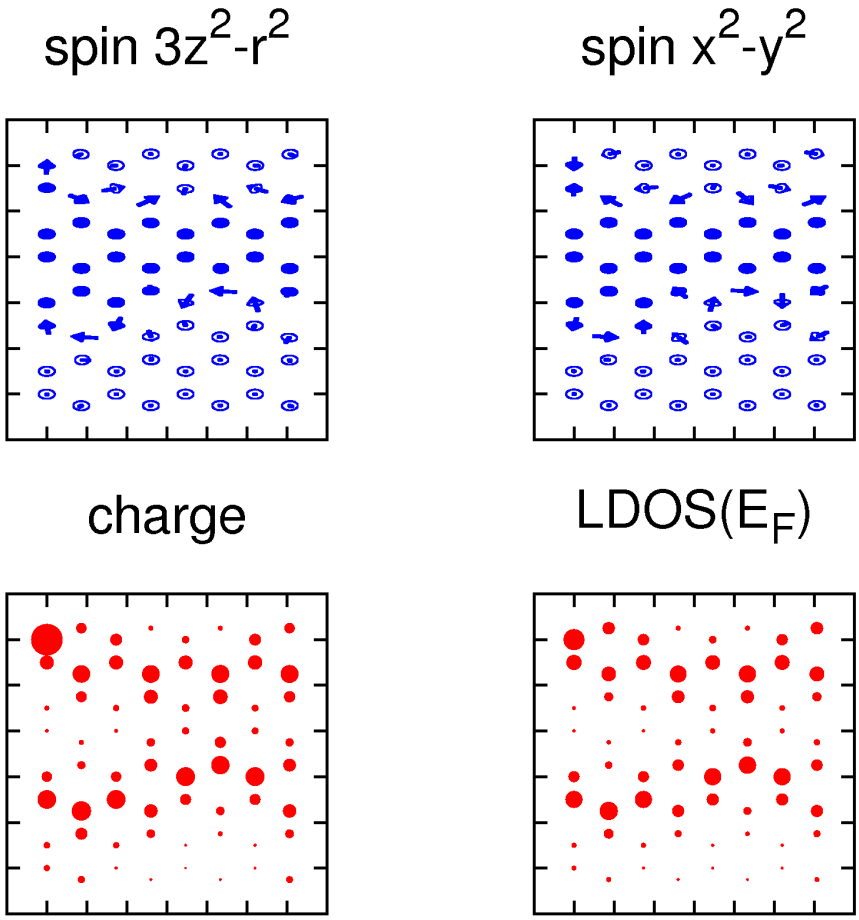

Figure 3.5: Spin in the $3z^2 - r^2$ orbital (upper left panel), the $x^2 - y^2$ orbital (upper right panel), doped charge (lower left panel) and LDOS(E_F) (lower right panel) at $U = 3.0$, $\lambda = 1.0$ when $n = 0.5625$.

Chapter 4

Two-orbital $t-J$ Model for the Iron-Pnictides

4.1 Introduction

The $t-J$ model has made considerable contributions to the studies of the cuprates[57], and hence a generalization applied to the iron-pnictides is certainly desired. According to the DFT calculations[85], most weight on the Fermi Surface (FS) of the iron-pnictides comes from the d_{xz} and d_{yz} orbitals, which are degenerate. For this reason, we derive out a $t-J$ model for the iron-pnictides with two degenerate orbitals.

4.2 Two-Orbital $t-J$ Model

We start with a two-orbital Hubbard model Hamiltonian (equation. 3.1). The spirit of the $t-J$ model for the cuprates is that the Hubbard repulsion on-site U is so large that two electrons can not sit in the same orbital. For this reason, let us define projection operators P_0,P_N,Q_0,Q_N, the definitions of which are:
P_0:Projects to the subspace in which the α orbital is not double occupied

P_N:Projects to the subspace in which the α orbital is double occupied

Q_0:Projects to the subspace in which the β orbital is not double occupied

Q_N:Projects to the subspace in which the β orbital is double occupied

And the spin configuration projectors T and W:

T means the low-energy spin configuration (e.g triplet for 2 electrons on one site) while W means the high-energy one.

Of course the spin projectors will only be useful in the case that none orbital is double occupied to a good approximation. Now we list the eigenstates of the interaction Hamiltonian for two electrons.

There are 3 triplets without double occupancy and energy $U^{'} - J$:

$$\begin{aligned} |1\rangle &= c^{\dagger}_{\alpha,\uparrow} c^{\dagger}_{\beta,\uparrow} |0\rangle \\ |2\rangle &= c^{\dagger}_{\alpha,\downarrow} c^{\dagger}_{\beta,\downarrow} |0\rangle \\ |3\rangle &= \frac{c^{\dagger}_{\alpha,\uparrow} c^{\dagger}_{\beta,\downarrow} + c^{\dagger}_{\alpha,\downarrow} c^{\dagger}_{\beta,\uparrow}}{\sqrt{2}} |0\rangle, \end{aligned} \tag{4.1}$$

1 singlet without double occupancy and energy $U^{'} + J = U - J$:

$$|4\rangle = \frac{c^{\dagger}_{\alpha,\uparrow} c^{\dagger}_{\beta,\downarrow} - c^{\dagger}_{\alpha,\downarrow} c^{\dagger}_{\beta,\uparrow}}{\sqrt{2}} |0\rangle, \tag{4.2}$$

the antisymmetric double occupied state with energy $U - J = U^{'} + J$:

$$|5\rangle = \frac{c^{\dagger}_{\alpha,\uparrow} c^{\dagger}_{\alpha,\downarrow} - c^{\dagger}_{\beta,\uparrow} c^{\dagger}_{\beta,\downarrow}}{\sqrt{2}} |0\rangle, \tag{4.3}$$

and the symmetric double occupied state with energy $U + J$:

$$|6\rangle = \frac{c^{\dagger}_{\alpha,\uparrow} c^{\dagger}_{\alpha,\downarrow} + c^{\dagger}_{\beta,\uparrow} c^{\dagger}_{\beta,\downarrow}}{\sqrt{2}} |0\rangle. \tag{4.4}$$

The projector P_0Q_0 will choose the non-double occupied states ($|1\rangle - - - -|4\rangle$). However, if we define a rotated basis:

$$\begin{aligned} c_\alpha^{'} &= \frac{c_\alpha + c_\beta}{\sqrt{(2)}}, \\ c_\beta^{'} &= \frac{c_\alpha - c_\beta}{\sqrt{(2)}}, \end{aligned} \tag{4.5}$$

and construct the state $|5^{'}\rangle = \frac{c_{\alpha,\uparrow}^{\dagger'} c_{\alpha,\downarrow}^{\dagger'} - c_{\beta,\uparrow}^{\dagger'} c_{\beta,\downarrow}^{\dagger'}}{\sqrt{2}}|0\rangle$ in the rotated basis, we will find that $|5^{'}\rangle = |4\rangle$. The physical reason for this is that the atomic orbitals, which are the eigenstates of a hydrogen-like atom, are not necessarily the eigenstates of electron-electron Coulomb interaction. In this two-orbital case, the H_4 term in the interaction Hamiltonian does not commute with the orbital particle number operator . So that an eigenstate of the interaction Hamiltonian with two electrons in different orbitals and net spin zero can have the two electrons sitting in the same orbital if we choose a rotated basis. Mathematically, this means that the projector P_0Q_0 is not invariant under a rotation, while the physics is certainly rotational invariant. For this reason, avoiding double occupied orbitals as done in the case of cuprates becomes impossible now. However, the projector TP_0Q_0, which will only keep the non-double occupied triplet states ($|1\rangle - - - -|3\rangle$), is invariant under basis rotation. This is expected from the simple fact that no other state is degenerate with these three. So now we are trying to find the effective Hamiltonian in the TP_0Q_0 subspace by a canonical transformation

$$K = e^{S^{'}} H e^{-S^{'}}. \tag{4.6}$$

We choose

$$\begin{aligned} H_0 &= WP_0Q_0HQ_0P_0W + TP_0Q_0HQ_0P_0T \\ &\quad + P_0Q_NHQ_NP_0 + P_NQ_0HQ_0P_N \\ &\quad + P_NQ_NHQ_NP_N \\ &\quad + (P_NQ_NHQ_0P_0 + H.C) \\ &\quad + (P_0Q_NHQ_0P_N + H.C), \\ H_1 &= H - H_0, \\ [H_0, S^{'}] &= H_1, \end{aligned} \tag{4.7}$$

and hence

$$K = H_0 + \frac{1}{2}[S^{'}, H_1] \tag{4.8}$$

$$\langle m|H_1|n\rangle = \langle m|H_0S^{'} - S^{'}H_0|n\rangle, \tag{4.9}$$

where $|m\rangle$ and $|n\rangle$ are the eigenstates of H_0. Then, we have

$$S^{'} = \sum_{m,n} |m\rangle\langle m|\frac{H_1}{E_m - E_n}|n\rangle\langle n|. \tag{4.10}$$

Now let us write H_1 out explicitly:

$$\begin{aligned} H_1 &= WP_0Q_0HQ_0P_0T + TP_0Q_0HQ_0P_0W \\ &\quad + (P_0Q_NHQ_NP_N + P_NQ_0HQ_NP_N) + H.C \\ &\quad + (TP_0Q_0HQ_NP_0 + WP_0Q_0HQ_NP_0) + H.C \\ &\quad + (TP_0Q_0HQ_0P_N + WP_0Q_0HQ_0P_N) + H.C. \end{aligned} \tag{4.11}$$

In the half-filling case, any hopping will lead a single occupied state to a double occupied state and the Hubbard terms can never modify a spin triplet into a spin singlet (or vice versa), so that the first line in the above equation vanishes. Many other

terms, in which both sides appear W or P_N or Q_N, will play no role in the effective Hamiltonian because the final Hamiltonian is projected in the subspace TP_0Q_0. For example, the term $WP_0Q_0HQ_NP_0$ will contribute in the following way

$$\begin{aligned} & TP_0Q_0[S^{'}, WP_0Q_0HQ_NP_0]Q_0P_0T \\ =& TP_0Q_0S^{'}WP_0Q_0HQ_NP_0Q_0P_0T - TP_0Q_0WP_0Q_0HQ_NP_0S^{'}Q_0P_0T. \end{aligned} \tag{4.12}$$

On the right hand side of the first term we see that $Q_NQ_0 = 0$ and on the left side of the second term we see $TW = 0$. In conclusion, we only need to count four terms in H_1 and can write $S^{'}$ as

$$\begin{aligned} S^{'} &= \sum_{m,n} |m\rangle\langle m| \frac{(TP_0Q_0HQ_NP_0 + TP_0Q_0HQ_0P_N) + H.C}{E_m - E_n} |n\rangle\langle n| \\ &= -\frac{(TP_0Q_0HQ_NP_0 + TP_0Q_0HQ_0P_N) - H.C}{U + J}. \end{aligned} \tag{4.13}$$

Now we are going to calculate $[S^{'}, H_1]$. Again, since the result still needs to be projected by TP_0Q_0 on each side, the terms with W or P_N or Q_N on any side will vanish and we do not need to count them. The result is:

$$\frac{1}{2}[S^{'}, H_1] = -\frac{TP_0Q_0H_{TB}(Q_NP_0 + P_NQ_0)H_{TB}Q_0P_0T}{U + J}, \tag{4.14}$$

where we replaced H by H_{TB}, which is the tight-binding hopping terms, because the interaction terms can not move electrons from a single occupied state to a double occupied one.

Now we express Q_0P_0T as $\sum_{S=0,1,2,M=-S...S} |1,1,S,M\rangle\langle 1,1,S,M|$ as the projectors will only keep triplet states, where S is the total spin of the nearby two sites and M is the z componetn of the total spin . However, the effect of the operators in H_{TB} is better described in the basis $|1, M_{\mathbf{i}}, 1, M_{\mathbf{j}}\rangle$ because the creation and annihilation operators are labeled by $\mathbf{i}$ and σ, which are the site and the z component of the local spin instead of the total spin. It is therefore straightforward to transform by the CG

coefficients:

$$\begin{aligned}
&\sum_{S=0,1,2,M=-S...S} |1,1,S,M\rangle\langle 1,1,S,M| \\
&= \sum_{S=0,1,2,M=-S...S} \sum_{M_{\mathbf{i}}=0,\pm1,M_{\mathbf{j}}=0,\pm1} |1,M_{\mathbf{i}},1,M_{\mathbf{j}}\rangle\langle 1,M_{\mathbf{i}},1,M_{\mathbf{j}}|1,1,S,M\rangle\langle 1,1,S,M| \\
&= \sum_{S=0,1,2,M=-S...S} \sum_{M_{\mathbf{i}}=0,\pm1,M_{\mathbf{j}}=0,\pm1} |1,M_{\mathbf{i}},1,M_{\mathbf{j}}\rangle C^{SM}_{1,M_{\mathbf{i}},1,M_{\mathbf{j}}}\langle 1,1,S,M|.
\end{aligned} \tag{4.15}$$

The intermediate state can be addressed by

$$Q_N P_0 + P_N Q_0 = \sum_{m_{\mathbf{i}}=\pm\frac{1}{2},m_j=\pm\frac{1}{2}} |\frac{1}{2},m_{\mathbf{i}},\frac{1}{2},m_{\mathbf{j}}\rangle\langle\frac{1}{2},m_{\mathbf{i}},\frac{1}{2},m_{\mathbf{j}}| \tag{4.16}$$

So that the numerator in equation (4.14) can be written as:

$$\sum_{S=0,1,2}^{M=-S...S} |1,1,S,M\rangle \sum_{m_{\mathbf{i}}=\pm\frac{1}{2},m_{\mathbf{j}}=\pm\frac{1}{2}} (\langle\frac{1}{2},m_{\mathbf{i}},\frac{1}{2},m_{\mathbf{j}}|H_t|1,M_{\mathbf{i}},1,M_{\mathbf{j}}\rangle C^{SM}_{1,M_{\mathbf{i}},1,M_{\mathbf{j}}})^2\langle 1,1,S,M|, \tag{4.17}$$

and

$$\begin{aligned}
\langle\frac{1}{2},m_{\mathbf{i}},\frac{1}{2},m_{\mathbf{j}}|H_{TB}|1,M_{\mathbf{i}},1,M_{\mathbf{j}}\rangle &= \langle\frac{1}{2},m_{\mathbf{i}},\frac{1}{2},m_{\mathbf{j}}|\sum_{\sigma}^{\alpha\beta} t^{\alpha\beta}_{\mathbf{i},\mathbf{j}} c^{\dagger}_{\mathbf{i},\sigma} c_{\mathbf{j},\sigma}|1,M_{\mathbf{i}},1,M_{\mathbf{j}}\rangle \\
&= \sum_{\sigma}^{\alpha\beta} t^{\alpha\beta}_{\mathbf{i},\mathbf{j}} C^{\frac{1}{2},m_{\mathbf{i}}}_{\frac{1}{2},\sigma,1,M_{\mathbf{i}}} C^{1,M_{\mathbf{j}}}_{\frac{1}{2},-\sigma,\frac{1}{2},m_{\mathbf{j}}}.
\end{aligned} \tag{4.18}$$

Then the numerator in equation (4.14) becomes

$$\sum_{S=0,1,2}^{M=-S...S} |1,1,S,M\rangle \sum_{m_{\mathbf{i}}=\pm\frac{1}{2},m_{\mathbf{i}}=\pm\frac{1}{2}} (\sum_{\sigma}^{\alpha\beta} t^{\alpha\beta}_{\mathbf{i},\mathbf{j}} C^{\frac{1}{2},m_{\mathbf{i}}}_{\frac{1}{2},\sigma,1,M_{\mathbf{i}}} C^{1,M_{\mathbf{j}}}_{\frac{1}{2},-\sigma,\frac{1}{2},m_{\mathbf{j}}} C^{SM}_{1,M_{\mathbf{i}},1,M_{\mathbf{j}}})^2\langle 1,1,S,M|. \tag{4.19}$$

By looking up the CG coefficient table and adding up all of them according to the above equation, we get the super exchange Hamiltonian

$$H_{SE} = \frac{2(t_1^2 + t_2^2)}{3(U+J)}(\mathbf{S_i} \cdot \mathbf{S_j} - 1) \tag{4.20}$$

for nearest neighbors, and

$$H_{SE} = \frac{4(t_3^2 + t_4^2)}{3(U+J)}(\mathbf{S_i} \cdot \mathbf{S_j} - 1) \tag{4.21}$$

for next nearest neighbors.

Our group and other collaborators performed Lanczos calculations using this model. More details can be found in ref. [1]

Chapter 5

Other Publications

In this chapter, all of my publications that are not described above are listed and their abstracts are also present, according to time order.

(1). *Highly anisotropic resistivities in the double-exchange model for strained manganites*, Shuai Dong, Seiji Yunoki, Xiaotian Zhang, Cengiz Sen, J.-M. Liu, Elbio Dagotto. Phys. Rev. B **82** 035118 (2010).

Abstract: The highly anisotropic resistivities in strained manganites are theoretically studied using the two-orbital double-exchange model. At the nanoscale, the anisotropic double-exchange and Jahn-Teller distortions are found to be responsible for the robust anisotropic resistivities observed here via Monte Carlo simulations. An unbalance in the population of orbitals caused by strain is responsible for these effects. In contrast, the anisotropic superexchange is found to be irrelevant to explain our results. Our model study suggests that highly anisotropic resistivities could be present in a wide range of strained manganites, even without (sub)micrometer- scale phase separation. In addition, our calculations also confirm the formation of anisotropic clusters in phase-separated manganites, which magnifies the anisotropic resistivities.

(2).*Microscopic model for the ferroelectric field effect in oxide heterostructures*,Shuai Dong, Xiaotian Zhang, Rong Yu, J.-M. Liu, and Elbio Dagotto, Phys. Rev. B **84** 155117 (2011).

Abstract: A microscopic model Hamiltonian for the ferroelectric field effect is introduced for the study of oxide heterostructures with ferroelectric components. The long-range Coulomb interaction is incorporated as an electrostatic potential, solved self-consistently together with the charge distribution. A generic double-exchange system is used as the conducting channel, epitaxially attached to the ferroelectric gate. The observed ferroelectric screening effect, namely, the charge accumulation/depletion near the interface, is shown to drive interfacial phase transitions that give rise to robust magnetoelectric responses and bipolar resistive switching, in qualitative agreement with previous density functional theory calculations. The model can be easily adapted to other materials by modifying the Hamiltonian of the conducting channel, and it is useful in simulating ferroelectric field effect devices particularly those involving strongly correlated electronic components where *ab initio* techniques are difficult to apply.

(3).*Properties of the multiorbital Hubbard models for the iron-based superconductors*,Elbio Dagotto, Adriana Moreo, Andrew Nicholson, Qinglong Luo, Shuhua Liang, Xiaotian Zhang, Front. Phys., **6(4)**, 379-397 (2011).

Abstract: A brief review of the main properties of multiorbital Hubbard models for the Fe-based superconductors is presented. The emphasis is on the results obtained by our group at the University of Tennessee and Oak Ridge National Laboratory, Tennessee, USA, but results by several other groups are also discussed. The models studied here have two, three, and five orbitals, and they are analyzed using a variety of computational and mean-field approximations. A physical region where the properties of the models are in qualitative agreement with neutron scattering, photoemission, and transport results is revealed. A variety of interesting open questions are briefly discussed such as: what are the dominant pairing tendencies in Hubbard models? Can

pairing occur in an interorbital channel? Are nesting effects of fundamental relevance in the pnictides or approaches based on local moments are more important? What kind of magnetic states are found in the presence of iron vacancies? Can charge stripes exist in iron-based superconductors? Why is transport in the pnictides anisotropic? The discussion of results includes the description of these and other open problems in this fascinating area of research.

Chapter 6

Conclusions

The research work that the author has done on strongly correlated electrons in order to apply for a Ph. D. degree from The University of Tennessee, Knoxville was illustrated above. We see that electron-electron interaction can explain several phenomenas that can not be understood by single-electron pictures.

In the iron-pnictides, the experimentally observed C type anti-ferromagnetism certainly breaks the D_{4h} lattice symmetry. Although the structural transition itself breaks the D_{4h} symmetry already, it appears to be too small to be counted as the main origin of the magnetic structure. The two-orbital $t-J$ model and corresponding Lanczos calculation[1], as well as other multi-orbital Hubbard model based mean-field calculations (for example, see Ref. [78]) show that the desired magnetic structure can easily emerge out of electron-electron interaction via spontaneous symmetry breaking. In consequence, the C_{4v} symmetry of the two-dimensional Fermi surface must be also destroyed by this symmetry breaking. We found that, although the conductivity along the anti-ferromagnetic direction is suppressed by Hund coupling as one would expect from a very intuitive point of view, this distortion of the Fermi surface suppresses the conductivity along the ferromagnetic direction even more. In conclusion, our work shows that the anisotropy of both the magnetic structure and the optical conductivity

of the iron-pnictides can be a result of the spontaneous symmetry breaking induced by the electron-electron interaction.

In the perovskite [111] bilayers, the flat energy band and the anomalous quantum Hall effect have been studied from the perspective of single-electron physics for a long time, because single-electron Hamiltonian (including the relativistic spin-orbital coupling term) is already enough to explain such effects. However, we have discovered that, when the energy band is flat enough, the electron-electron interaction can produce a Chern insulator out of a band insulator. This is also realized through spontaneous symmetry breaking. What gives the Hall conductance to a Chern insulator is the spin-orbital coupling $\mathbf{l} \cdot \mathbf{s}$, and hence the system shows no Hall conductance if there is no net magnetization. As soon as the Coulomb repulsion between electrons spontaneously breaks the $SU(2)$ symmetry of the electron spin and turns the system into a magnet, a Hall conductance naturally is produced.

Electron-electron interaction induced spontaneous symmetry breaking is interesting and challenging, especially in today's widely studied systems such as high temperature superconductors and topological insulators. Although my research has explored only a small corner of this field, hopefully it made interesting contributions. I believe that additional research by other physicist will substantially help in deciding of our predictions are or not realized in nature.

Bibliography

Bibliography

[1] A. Nicholson, W. Ge, X. Zhang, J. Riera, M. Daghofer, A. M. Oles, G. B. Marthins, A. Moreo, and E. Dagotto, Phys. Rev. Lett. **106**, 217002 (2011). v, 60, 64

[2] Y. Kamihara, T. Watanabe, M. Hirano, and H. Hosono, J. of the Am. Chem. Soc. **130**, 3296 (2008). 1

[3] G. F. Chen, Z. Li, G. Li, J. , D. Wu, J. Dong, W. Z. Hu, P. Zheng, Z. J. Chen, H. Q. Yuan, J. Singleton, J. L. Luo, and N. L. Wang, Phys. Rev. Lett. **101**, 057007 (2008). 1

[4] G. F. Chen, Z. Li, D. Wu, G. Li, W. Z. Hu, J. Dong, P. Zheng, J. L. Luo, and N. L. Wang, Phys. Rev. Lett. **100**, 247002 (2008). 1

[5] X. H. Chen, T. Wu, G. Wu, R. H. Liu, H. Chen, and D. F. Fang, Nature **453**, 761 (2008). 1

[6] Z.-A. Ren, W. Lu, J. Yang, W. Yi, X.-L. Shen, Z.-C. Li, G.-C. Che, X.-L. Dong, L.-L. Sun, F. Zhou, and Z.-X. Zhao, Chin. Phys. Lett. **25**, 2215 (2008). 1

[7] Z.-A. Ren, G.-C. Che, X.-L. Dong, J. Yang, W. Lu, W. Yi, X.-L. Shen, Z.-C. Li, L.-L. Sun, F. Zhou, and Z.-X. Zhao, EPL **83**, 17002 (2008). 1

[8] D. C. Johnston, arXiv:1005.4392. 1, 5

[9] K. Haule, J. H. Shim, and G. Kotliar, Phys. Rev. Lett. **100**, 226402 (2008). 1

[10] L. Boeri, O. V. Dolgov, and A. A. Golubov, Phys. Rev. Lett. **101**, 026403 (2008). 1

[11] A. D. Christianson, M. D. Lumsden, O. Delaire, M. B. Stone, D. L. Abernathy, M. A. McGuire, A. S. Sefat, R. Jin, B. C. Sales, D. Mandrus, E. D. Mun, P. C. Canfield, J. Y. Y. Lin, M. Lucas, M. Kresch, J. B. Keith, B. Fultz, E. A. Goremychkin, and R. J. McQueeney Phys. Rev. Lett. **101**, 157004 (2008). 1

[12] C. Wang , L. Li , S. Chi , Z. Zhu , Z. Ren , Y. Li , Y. Wang , X. Lin , Y. Luo , S. Jiang , X. Xu , G. Cao and Z. Xu, EPL **83**, 67006 (2008). 1

[13] J. W. Lynn and P. Dai, Physica C **469**, 469 (2009); and references therein. x, 1, 4, 5, 6

[14] M. D. Lumsden and A. D. Christianson, J. Phys.: Condens. Matter **22** 203203 (2010). x, 1, 2, 3

[15] C. Cao, P. J. Hirschfeld, and H.-P. Cheng, Phys. Rev. B **77**, 220506(R) (2008); and references therein. 2

[16] Joshua H. Tapp, Zhongjia Tang, Bing Lv, Kalyan Sasmal, Bernd Lorenz, Paul C.W. Chu, Arnold M. Guloy, Phys. Rev. B **78** 060505(R) (2008). 4

[17] S. Li *et al.*, Phys. Rev. B **08**, 020504 (2009). x, 3, 4

[18] C. de la Cruz, Q. Huang, J.W. Lynn, J. Li, W. Ratcliff II, J.L. Zarestky, H.A. Mook, G.F. Chen, J.L. Luo, N.L. Wang, P. Dai, Nature (london) **453**, 899 (2008). 4

[19] C.H. Lee, A. Iyo, H. Eisaki, H. Kito, M.T. Fernandez-Diaz, T. Ito, K. Kihou, H. Matsuhata, M. Braden, K. Yamada, J. Phys. Soc. Jpn. **77** 083704 (2008). 4

[20] M.A. McGuire, A.D. Christianson, A.S. Sefat, B.C. Sales, M.D. Lumsden, R. Jin, E.A. Payzant, D. Mandrus, Y. Luan, V. Keppens, V. Varadarajan, J.W.

Brill, R.P. Hermann, M.T. Sougrati, F. Grandjean, G.J. Long, Phys. Rev. B **78** 094517 (2008). 4

[21] Q. Huang, J. Zhao, J.W. Lynn, G.F. Chen, J.L. Lou, N.L. Wang, P. Dai, Phys. Rev. B **78** 054529 (2008). 4

[22] M. Ishikado, R. Kajimoto, S. Shamoto, M. Arai, A. Iyo, K. Miyazawa, P. M. Shirage, H. Kito, H. Eisaki, S.-W. Kim, H. Hosono, T. Guidi, R. Bewley, S.M. Bennington, arxiv: 0809.5128v2. 4

[23] J. Zhao, Q. Huang, C. de al Cruz, S. Li, J.W. Lynn, Y. Chen, M.A. Green, G.F. Chen, G. Li, Z.C. Li, J.L. Luo, N.L. Wang, P. Dai, Nature Mater. **7** 953-959 (2008). x, 4, 5, 7

[24] Y. Chen, J.W. Lynn, J. Li, G. Li, G.F. Chen, J.L. Luo, N.L. Wang, P. Dai, C. dela Cruz, H.A. Mook, Phys. Rev. B **78** 064515 (2008). 4

[25] Y. Qiu, W. Bao, Q. Huang, T. Yildirim, J.M. Simmons, M.A. Green, J.W. Lynn, Y.C. Gasparovic, J. Li, T. Wu, G. Wu, X.H. Chen, Phys. Rev. Lett. **101** 257002 (2008). 4

[26] J. Zhao, Q. Huang, Clarina de la Cruz, J.W. Lynn, M.D. Lumsden, Z.A. Ren, J. Yang, X. Shen, X. Dong, Z. Zhao, P. Dai, Phys. Rev. B **78** 132504 (2008). 4

[27] S.A.J. Kimber, D.N. Argyriou, F. Yokaichiya, K. Habicht, S. Gerischer, T. Hansen, T. Chatterji, R. Klingeler, C. Hess, G. Behr, A. Kondrat, B. Buchner, Phys. Rev. B **78** 140503 (2008). 4

[28] J. Zhao, W. Ratcliff-II, J.W. Lynn, G.F. Chen, J.L. Luo, N.L. Wang, J. Hu, P. Dai, Phys. Rev. B **78** 140504(R) (2008). 4

[29] K. Kaneko, A. Hoser, N. Caroca-Canales, A. Jesche, C. Krellner, O. Stockert, C. Geibel, Phys. Rev. B **78** 212502 (2008). 4

[30] A. Jesche, N. Caroca-Canales, H. Rosner, H. Borrmann, A. Ormeci, D. Kasinathan, H.H. Klauss, H. Luetkens, R. Khasanov, A. Amato, A. Hoser, K. Kaneko, C. Krellner, C. Geibel, Phys. Rev. B **78** 180504 (2008). 4

[31] A.I. Goldman, D.N. Argyriou, B. Ouladdiaf, T. Chatterji, A. Kreyssig, S. Nandi, N. Ni, S.L. Bud'ko, P.C. Canfield, R.J. McQueeney, Phys. Rev. B **78** 100506(R) (2008). 4

[32] A. Kreyssig, M.A. Green, Y.B. Lee, G.D. Samolyuk, P. Zajdel, J.W. Lynn, S.L. Bud'ko, M.S. Torikachvili, N. Ni, S. Nandi, J. Leao, S.J. Poulton, D.N. Argyriou, B.N. Harmon, P.C. Canfield, R.J. McQueeney, A.I. Goldman, Phys. Rev. B **78** 184517 (2008). 4

[33] A.I. Goldman, A. Kreyssig, K. Prokes, D.K. Pratt, D.N. Argyriou, J.W. Lynn, S. Nandt, S.A. Kimber, Y. Chen, Y.B. Lee, G. Samolyuk, J. Leao, S.J. Poulton, S.L. Bud'ko, N. Ni, P.C. Canfield, B.N. Harmon, R.J. McQueeney, Phys. Rev. B **79** 024513 (2009). 4

[34] Q. Huang, Y. Qiu, W. Bao, J.W. Lynn, M.A. Green, Y.C. Gasparovic, T. Wu, G. Wu, X.H. Chen, Phys. Rev. Lett. **101** 257003 (2008). 4

[35] M. Kofu, Y. Qiu, Wei Bao, S.-H. Lee, S. Chang, T. Wu, G. Wu, X.H. Chen, New J. Phys. **11** 055001 (2009). 4

[36] Y. Su, P. Link, A. Schneidewind, Th. Wolf, P. Adelmann, Y. Xiao, M. Meve, R. Mittal, M. Rotter, D. Johrendt, Th. Brueckel, M. Loewenhaupt, Phys. Rev. B **79** 064504 (2009). 4

[37] H. Luetkens, H.-H. Klauss, M. Kraken, F. J. Litterst, T. Dellmann, R. Klingeler, C. Hess, R. Khasanov, A. Amato, C. Baines, M. Kosmala, O. J. Schumann, M. Braden, J. Hamann-Borrero, N. Leps, A. Kondrat, G. Behr, J. Werner and B. Buchner, Nature Materials **8**, 305-309 (2009). 5

[38] C. R. Rotundu, D. T. Keane, B. Freelon, S. D. Wilson, A. Kim, P. N. Valdivia, E. Bourret-Courchesne, R. J. Birgeneau, arXiv:0907.1308v1. 5

[39] A. J. Drew, Ch. Niedermayer, P. J. Baker, F. L. Pratt, S. J. Blundell, T. Lancaster, R. H. Liu, G. Wu, X. H. Chen, I. Watanabe, V. K. Malik, A. Dubroka, M. Rossle, K. W. Kim, C. Baines and C. Bernhard, Nature Materials **8**, 310-314 (2009). 5

[40] Serena Margadonna, Yasuhiro Takabayashi, Martin T. McDonald, Michela Brunelli, G. Wu, R. H. Liu, X. H. Chen, and Kosmas Prassides, Phys. Rev. B **79**, 014503 (2009). 5

[41] Jiun-Haw Chu, James G. Analytis, Chris Kucharczyk, and Ian R. Fisher, Phys. Rev. B **79**, 014506 (2009). 5

[42] R. Khasanov, M. Bendele, A. Amato, P. Babkevich, A. T. Boothroyd, A. Cervellino, K. Conder, S. N. Gvasaliya, H. Keller, H.-H. Klauss, H. Luetkens, V. Pomjakushin, E. Pomjakushina, and B. Roessli, Phys. Rev. B **80**, 140511(R) (2009). 5

[43] E. Dagotto, T. Hotta, and A. Moreo, Physics Reports **344**, 1 (2001). 6

[44] Y. Tokura, Fundamental features of colossal magnetoresistive manganese oxides. In: Tokura, Y. (Ed.), Contribu-tion to Colossal Magnetoresistance Oxides, Monographs in Condensed Matter Science. Gordon & Breach, London (1999). xi, 7, 8

[45] E. O. Wollan, W. C. Koehler, Phys. Rev. **100**, 545 (1955). xi, 7

[46] F. D. M. Haldane, Phys. Rev. Lett. **61**, 2015 (1988). 10, 42

[47] C. L. Kane and E. J. Mele, Phys. Rev. Lett. **95**, 146802 (2005). 10, 42

[48] B. A. Bernevig, T. L. Hughes, and S.-C. Zhang, Science **314**, 17571761 (2006). 10, 42

[49] J. E. Moore, and L. Balents, Phys. Rev. B **75**,121306 (2007). 10, 42

[50] L. Fu, C. L. Kane, and E. J. Mele, Phys. Rev. Lett. **98**, 106803 (2007). 10, 42

[51] M. König *et al.* Science **318**, 766770 (2007). 10, 42, 43

[52] D. Hsieh *et al.*, Nature **452**, 970974 (2008). 10, 42, 43

[53] Y. Xia *et al.*, Nature Phys. **5**, 398402 (2009). 10, 42, 43

[54] Noh, H.-J. *et al.*, Europhys. Lett. **81**, 57006 (2008). 10, 42, 43

[55] G. Wang *et al.*, Nano Res. **3**, 874 (2010). 10, 42, 43

[56] Di Xiao, Wenguang Zhu, Ying Ran, Naoto Nagaosa and Satoshi Okamoto, Nat. Commun. **2**, 596 (2011). xi, 9, 11, 43, 44, 46

[57] E. Dagotto., Rev. Mod. Phys **66**, 763 (1994). ix, 26, 33, 34, 41, 45, 54

[58] D. Wu *et al.*, arXiv:0912.3334. xi, 28, 29

[59] D. Wu *et al.*, arXiv:1011.1207. 28

[60] M. Nakajima *et al.*, arXiv:1003.5038. xi, 28

[61] N. L. Wang *et al.*, arXiv:1105.3939. xi, 28, 29, 30

[62] N. Barisic *et al.*, arXiv:1004.1658. 28

[63] J. J. Tu *et al.*, arXiv:1008.3908. 28

[64] R. H. Yuan *et al.*, arXiv:1102.1381. 28

[65] Taichi Terashima *et al.*, J. Phys. Soc. Jpn **78**, 063702 (2009). 28

[66] M. Nakajima *et al.*, J. Phys. Chem. Solids (2010), doi:10.1016/j.jpcs.2010.10.049. 28

[67] M. Dressel *et al.*, J. Phys. Chem. Solids (2010), doi:10.1016/j.jpcs.2010.10.004. 28

[68] M. A. Tanatar *et al.*, Phys. Rev. B **81**, 184508 (2010). 29

[69] J.-H. Chu *et al.*, Science **329**, 824 (2010). xi, 29, 30, 31

[70] D. C. Johnston, Adv. Phys. **59**, 803 (2010). 31

[71] For a recent review see I. R. Fisher, L. Degiorgi, and Z. X. Shen, arXiv:1106.1675. 31, 36

[72] E. C. Blomberg *at al.*, Phys. Rev. B **83**, 134505 (2011); and references therein. 31

[73] A. Dusza, A. Lucarelli, A. Sanna, S. Massidda, J.-H. Chu, I.R. Fisher, and L. Degiorgi arXiv:1107.0670. 32

[74] M. Daghofer, Q. L. Luo, R. Yu, D. X. Yao, A. Moreo, and E. Dagotto, Phys. Rev. B **81**, 180514(R) (2010). 32, 37, 39

[75] B. Valenzuela, E. Bascones, and M. J. Calderón, Phys. Rev. Lett. **105**, 207202 (2010). 32, 36, 37, 39

[76] K. Sugimoto, E. Kaneshita, and T. Tohyama, J. Phys. Soc. Jpn. **80**, 033706 (2011). 32, 36

[77] Density functional results are also compatible with experiments (J. Ferber, Johannes Ferber, Yu-Zhong Zhang, Harald O. Jeschke, and Roser Valenti Phys. Rev. B **82**, 165102 (2010)). 32

[78] Maria Daghofer, Andrew Nicholson, Adriana Moreo, and Elbio Dagotto, Phys. Rev. B **81**, 014511 (2010). ix, 32, 33, 36, 39, 64

[79] Qinlong Luo, George Martins, Dao-Xin Yao, Maria Daghofer, Rong Yu, Adriana Moreo, and Elbio Dagotto, Phys. Rev. B **82**, 104508 (2010). xii, 33, 35, 36, 37, 38

[80] Rong Yu, Kien T. Trinh, Adriana Moreo, Maria Daghofer, Jose Riera, Stephan Haas, and Elbio Dagotto, Phys. Rev. B **79**, 104510 (2009). 33

[81] A. Moreo, M. Daghofer, J. A. Riera, and E. Dagotto, Phys. Rev. B **79** 134502 (2009). 33

[82] A. Nicholson, Qinlong Luo, Weihao Ge, José Riera, Maria Daghofer, arXiv: 1107.2962. 39

[83] D. Akahoshi, M. Uchida, Y. Tomioka, T. Arima, Y. Matsui, and Y. Tokura, Phys. Rev. Lett **90**, 177203 (2003). 50

[84] S. Dong, X. Zhang, R. Yu, J.-M. Liu, and E. Dagotto, Phys. Rev. B **84**, 155117 (2011). 51

[85] S. Graser, T. A. Maier, P. J. Hirschfeld, and D. J. Scalapino, New J. Phys. **11**, 025016 (2009). 54

[86] A. R*ü*egg and G. A. Fiete, Phys. Rev. B **84**, 201103 (2011).

[87] T. Zhou *et al.*, arXiv:1102.2401.

[88] Y. F. Guo *et al.*, Phys. Rev. B **82**, 054506 (2010).

[89] Y. Li *et al.*, arXiv:1011.6008.

[90] M. Sato *et al.*, arXiv:0907.3007.

[91] T. Kaliyado *et al.*, arXiv:1004.5093.

[92] S. Onari *et al.*, Phys. Rev. Lett **103**, 177001 (2009).

[93] Y. Bang *et al.*, arXiv:1012.0414.

[94] S. Onari *et al.*, arXiv:1012.3307.

[95] T. Zhou *et al.*, arXiv:1105.1851.

[96] D. Zhang *et al.*, Phys. Rev. Lett **103**, 186402 (2009).

[97] M. Daghofer and A. Moreo, Phys. Rev. Lett **104**, 089701 (2010).

[98] Y. G. Pogorelov*et al.*, arXiv:1105.3608.

[99] R. M. Fernandes *et al.*, arXiv:1105.3906.

[100] R. B. Laughlin, Physical Review Letters **50**, 1395-1398 (1983).

[101] M. Hohenadler, T. C. Lang and F. F. Assaad, Arxiv 1011, 5063.

[102] Y. Yamaji and M. Imada, Arxiv 1012, 2637.

[103] Shun-Li Yu, X. C. Xie, and Jian-Xin Li, Arxiv 1101, 0911.

[104] Dung-Hai Lee, Arxiv 1105, 4900.

Vita

Xiaotian Zhang was born in 1986 in Beijing, the capital of the People's Republic of China. He had a happy childhood with his grandmother and mother, as well as plenty of friends. Xiaotian had his first physics class at 14 years old in middle school, and from that moment on he started to be interested in physics. Xiaotian obtained a Bachelor of Science degree with a physics major from Tsinghua University, Beijing, People's Republic of China in 2008, and came to the University of Tennessee, Knoxville and Oak Ridge National Laborary in the same year for his Ph. D. study in *Dr.* Elbio Dagotto's group.

In the first two years of his Ph. D. research Xiaotian focused on the manganites, from which he got two publications and learned the quantum Monte Carlo technique. But after that he decided to switch to the iron-pnictides and later topological insulators. Although it reduced the possible number of publications, this multi-material background gives him deeper understanding of condensed matter physics as well as the quantum mechanics behind it.